Composite Structures 330 (2024) 117840

Contents lists available at ScienceDirect

Composite Structures

journal homepage: www.elsevier.com/locate/compstruct

Quasi-3D free and forced vibrations of poroelastic microplates in the framework of modified couple stress theory

Behrouz Karami [a,*], Mergen H. Ghayesh [a], Nicholas Fantuzzi [b]

[a] School of Electrical and Mechanical Engineering, University of Adelaide, Adelaide, SA 5005, Australia
[b] Department of Civil, Chemical, Environmental, and Materials Engineering, University of Bologna, Bologna, Italy

ARTICLE INFO

Keywords:
Poroelastic microplates
Thickness stretching
Material imperfection
Free vibration
Forced vibration

ABSTRACT

In this study, a comprehensive study on the vibration behaviour of functionally graded thick microplates with material imperfections is presented for free and forced vibrations within a quasi-3D model and the modified couple stress (MCS) theory. Axial, transverse, rotation, and stretching motions are considered for modelling the thick microplate in the framework of the modified power-law scheme and quasi-3D and MCS theories. The microplate deformation is assumed to be infinitesimal and is modelled using the linear strain–displacement relationships. Using a virtual work method, the governing motion equations are derived. For fourfold coupled (axial-transverse-rotation-stretching) characteristics, the partial differential equations components are discretised via trigonometric expressions and the corresponding natural frequencies and time histories (time-dependent deflections) are determined numerically. The methodology and model are initially validated through a comparative analysis between the natural frequencies of the macrolevel simplified structure and those obtained using finite element software. Additionally, the simulation is compared, for validation purposes, with other simplified versions from the literature. Once model's validity is confirmed, an investigation into the quasi-3D free and forced vibrations of the structure is conducted for the new model. The results demonstrate the considerable effect of thickness stretching and material imperfection on the vibration characteristics of the poroelastic thick microplates.

1. Introduction

Microplates: Microsystems have become increasingly popular in a wide range of applications, thanks to their energy consumption, weight, and low cost, all of which have been greatly enhanced by recent technological developments. Microsystems have found notable applications in various fields, one of which is microelectromechanical systems (MEMSs) [1], encompassing resonators [2,3], actuators [4,5], energy harvesters [6], energy absorption [7], sensors [8], semiconductors [9], switches [10], and motors [11]. Furthermore, MEMS are widely employed in medicine [12], for instance, in the areas of neurology, urology, monitoring, diagnosis, surgery, cardiology, and drug delivery [13,14]. One of the fundamental elements utilised in the fabrication of MEMS is microplates [15,16]. In particular, microplates fabricated from functionally graded material (FGM) have attracted significant attention in the MEMS field recently [17–19], owing to the current advancements in micromachining for producing composite structures [20].

FGM structures: Recently, there has been a growing interest in inhomogeneous or non-uniform materials that exhibit continuously or logarithmically varying material properties in at least one direction [21–23], and differ from the way that geometric properties are varied to build up non-uniform structures [24,25], and is referred to as FGMs by scientists. FGMs are often combined of two distinct materials selected to achieve a target property or to optimise the performance of a particular device. These materials offer several advantages over homogeneous materials, including the ability to engineer materials with superior properties to suit engineering applications [26]. Despite the possibility of fabricating microstructures made of FGMs through advances in additive manufacturing techniques [27], this remains a costly option. That is why theoretical analysis of MEMS made of FGM has attracted significant attention [28–30], and is considered a critical element in the development of such microsystems.

Quasi-3D and miniature influences: There are various theories governing the static and dynamic status of continuous structures, such as beams, plates, and shells, considering the transverse shear effect. These theories include the first-, second-, and third-order shear deformation

* Corresponding author.
E-mail addresses: behrouz.karami@adelaide.edu.au (B. Karami), mergen.ghayesh@adelaide.edu.au (M.H. Ghayesh).

https://doi.org/10.1016/j.compstruct.2023.117840
Received 10 November 2023; Received in revised form 15 December 2023; Accepted 20 December 2023
Available online 22 December 2023

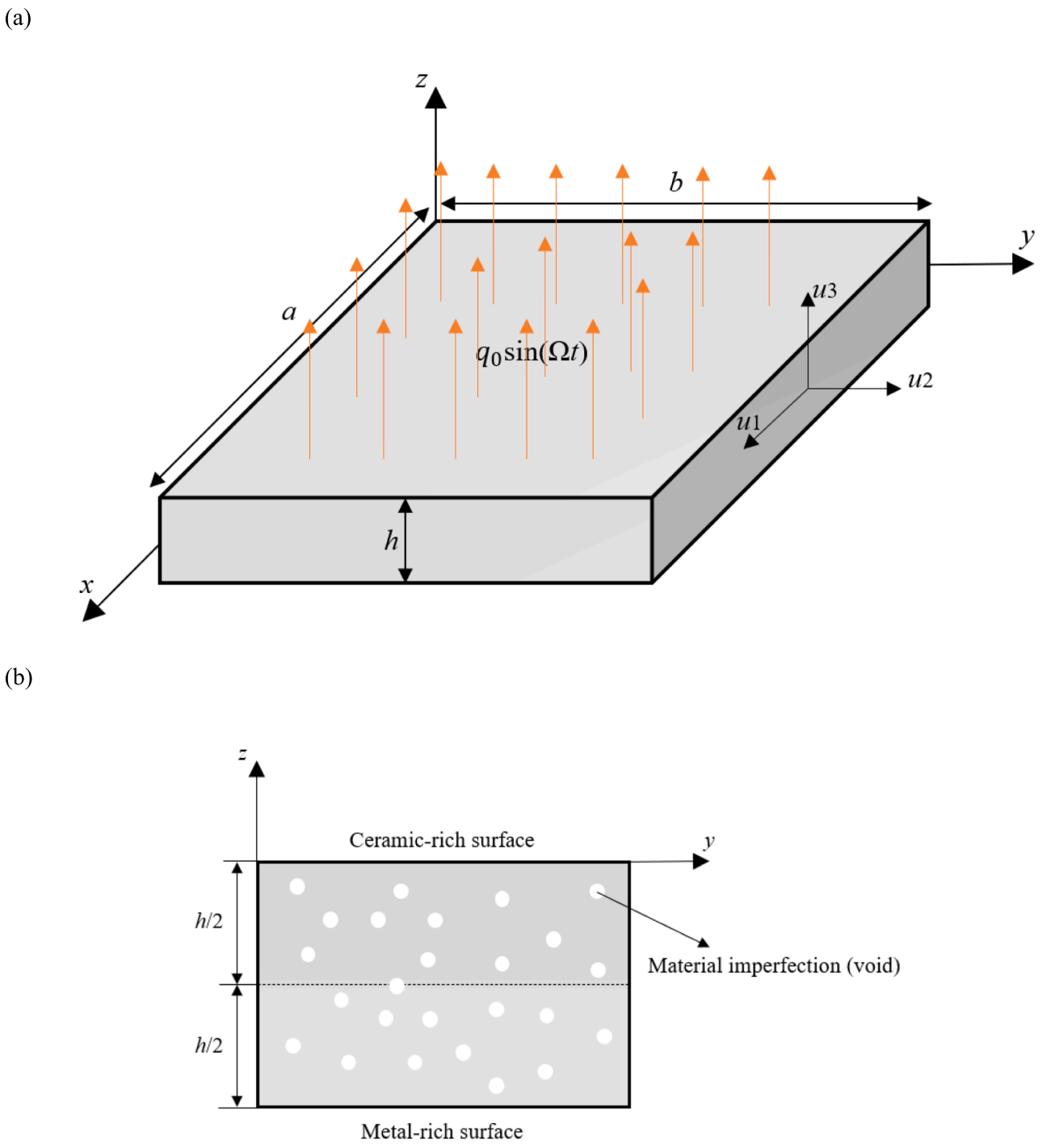

Fig. 1. A schematic of quasi-3D poroelastic thick microplate (a), and cross section of the microplate (b).

theories [31–33], and other refined high-order shear deformation theories, with and without considering the *thickness stretching* effect (via a quasi-3D model) to examine the mechanics of such structures under thermal and/or mechanical loads. Experimental observations have revealed that the mechanical characteristics of microstructures are size-dependent, resulting in alterations in their mechanical performance when compared to macrostructures. Moreover, regardless of the type of classical (scale-independent) theories, the application of classical continuum mechanics to investigate these properties can be inaccurate. Hence, researchers have focused on the theoretical development to incorporate small-scale influences in the framework of nonclassical theories. The MCS theory has been proposed to incorporate the size and has widely been used in various investigations [34–36]. This theory aims to consider the influence of small-scale effects on the behaviour of structures, which is particularly relevant for microstructures.

Porosity: Material imperfections or porosities (micro-voids) are one of the common imperfections seen in FGM fabrication because of material build-up due to manufacturing challenges, operation, or technical problems over time. For instance, research conducted by Zhu et al. [37] demonstrated that shrinkages may arise between adjacent compositions

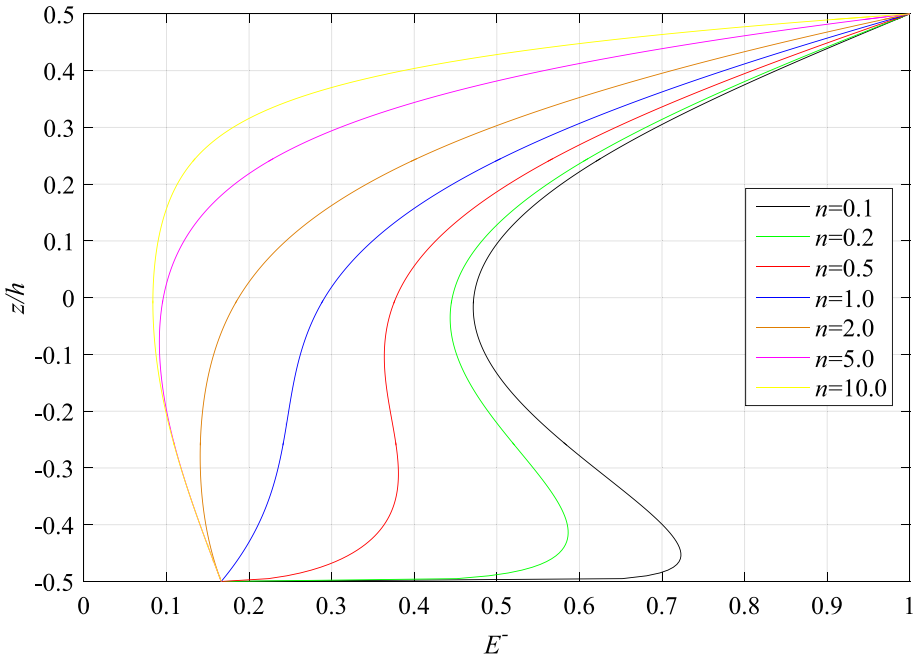

Fig. 2. Variation of Young's modulus through z-axis, ($\overline{E} = E(z)/E_c, \phi = 0.50$), based on the formulation from Ref. [59].

of metal and ceramic phases during the sintering process of FGMs, which could result in the formation of porosities within the material. Furthermore, when employing the multi-step sequential infiltration technique to produce FGMs, the porosities were predominantly found in the middle zone of the FGM structures due to the difficulty in fully infiltrating the secondary material into this zone, as compared to the top and bottom zones where infiltration was simpler and left fewer porosities [38]. Consequently, considering porosity influences on the mechanics of engineering structures composed of FGMs is important. Scientists have attempted to develop models that account for porosity; for instance, Wattanasakulpong and Chaikittiratana [39] proposed a modified power-law rule that incorporates porosity volume fraction as a parameter. To date, there are many investigations have been devoted to understanding the mechanics of imperfect FGMs in both macro and submicron structures. Briefly reviewing *macro*scale FGMs considering voids, in a recent study presented by Kumar et al. [40], a meshfree technique on dynamics and stability analyses of heterogeneous plates was developed. Rezaei et al. [41] analysed the free vibration behaviour of FGM plates with porosities via a refined higher-order shear deformable model. A detailed study on the oscillation characteristics of FGM plates with variable thickness and porosities can be found in Ref. [42]. In some recent studies, the free oscillation analysis of FGM plates and shells considering material imperfections has been investigated by Su et al. [43,44]. There have been some studies in the literature which focused on the effect of viscosity; for example, free vibration and damping analyses of porous FGM multi-layered plates with a viscoelastic core has been studied by Zhang et al. [45]. Liang and Wang [46] studied the viscoelastic wave characteristics of FGM multi-layered plates with porosities. Dynamic response of viscoelastic FGM beams with porosities under pulse load has been assessed by Akbas et al. [47]. Allah and Timesli [48] examined the nonlinear dynamics of viscoelastic FGM plates with linear and nonlinear porosity distributions. Downsizing to *nano/microstructures*, Shojaeefard et al. [49] investigated both vibrations and thermal buckling analyses of FGM plates with material imperfections. Mirjavadi et al. [50] assessed the dynamics of heterogeneous microshells of cylindrical shape with porosities under a moving load. The results demonstrate that the strain gradients, porosity

Table 1
Comparison of natural frequencies (Hz) of an isotropic *macro*plates.

(*m*,*n*)	Formula	ANSYS [67]	Discrepancy (%)
(1,1)	494.4296	492.4218	0.41
(1,2)	1235.3997	1232.172	0.26
(2,1)	1235.3997	1232.172	0.26
(2,2)	1975.5630	1967.460	0.41
(1,3)	2468.5581	2464.870	0.15
(3,1)	2468.5581	2464.870	0.15
(2,3)	3207.3821	3196.093	0.35
(3,2)	3207.3821	3196.093	0.35
(1,4)	4191.2362	4187.344	0.09
(4,1)	4191.2362	4187.344	0.09

percentage, and velocity of moving load, alter forced vibration characteristics of the system largely. Phung-Van et al. [51] examined the porosity-dependent nonlinear transient behaviour of FGM nanoscale plates via an isogeometric analysis. Chen et al. [52] studied the nonlinear bending behaviour of imperfect composite microplates with a central cut-out using isogeometric finite element modelling. Guo et al. [53] analysed the dynamic behaviour of porous FGM microplates on an elastic foundation under moving load with acceleration. There have also been studies in the literature that included the effect of viscosity; for example, Farokhi and Ghayesh [54] highlighted that the viscoelastic property highly affects the resonant position of viscoelastic imperfect microbeams. Jalaei and Civalek [55] studied the instability of magnetically viscoelastic FGM nanobeams with porosities. Moving-load excited response of imperfect FGM nanoplates resting on viscoelastic foundation has been studied by Liu et al. [56].

To date, the available research has not considered *quasi-3D free and forced vibrations* of *poroelastic* microplates in the *framework of MCS theory* (for example see Refs. [57,58]). Therefore, the current research study addresses this gap and presents the effects of thickness stretching and the length scale parameter on the natural frequencies and time histories (time-dependent deflection) in moderately thick and thick poroelastic microplates. More specifically, via use of MCS theory which incorporates miniature size effects, a quasi-3D model of the microplate is developed. This manuscript is organised as follows: Section 2 presents

Table 2
Dimensionless natural frequencies ($\widehat{\omega}_{mn} = \omega_{mn}h\sqrt{\rho/G}$) of isotropic square *macro*plate, ($a = 10$, $b/a = 1$, $h/a = 0.10$, $E = 30$ MPa, $\rho = 1$ kg/m^3, $\nu = 0.3$).

Model	(*m*,*n*)						
	(1,1)	(1,2)	(2,2)	(2,3)	(3,3)	(2,4)	(1,5)
Zhou et al. [68]	0.0932	0.2226	0.3421	0.5239	0.6889	0.7511	0.9268
Jha et al. [69]	0.0932	0.2226	0.3421	0.5240	0.6892	0.7515	0.9275
Benahmed et al. [70]	0.0932	0.2229	0.3425	0.5248	0.6904	0.7528	0.9294
Current study	0.0932	0.2226	0.3421	0.5241	0.6892	0.7515	0.9275

Table 3
Dimensionless fundamental frequency of perfect FGM square microplates, ($E_c = 14.4$ GPa, $E_m = 1.44$ GPa, $\rho_c = 12200$ kg/m^3, $\rho_m = 1220$ kg/m^3, $\nu = 0.38$, $h = 17.6$ μm, $b/a = 1$).

n	*a*/*h*	Model	ℓ/h				
			0.0	0.2	0.4	0.6	0.8
0	5	Thai et al. [71]	5.9671	6.3957	7.5366	9.1264	10.9718
		Jung et al. [72]	5.3871	5.7797	6.7996	8.1595	9.6451
		Current study	5.4216	5.8446	6.9600	8.4968	10.2640
	10	Thai et al. [71]	6.1103	6.5491	7.7174	9.3453	11.2349
		Jung et al. [72]	5.9301	6.3559	7.4807	9.0261	10.7848
		Current study	5.9413	6.3774	7.5357	9.1456	11.0105
1	5	Thai et al. [71]	5.2960	5.7810	7.0383	8.7406	10.6773
		Jung et al. [72]	4.8744	5.3239	6.4600	7.9298	9.4998
		Current study	5.0830	5.5396	6.7245	8.3292	10.1519
	10	Thai et al. [71]	5.3953	5.8894	7.1702	8.9045	10.8775
		Jung et al. [72]	5.2697	5.7518	6.9920	8.6477	10.942
		Current study	5.5019	5.9729	7.2032	8.8824	10.8027

the modified power-law rule of mixtures, kinematic fields, proposed plate theory, MCS constitutive equation and equilibrium expression of the proposed model. Section 3 explains on the solution procedure and numerical solutions for simply supported boundary condition by using a set of trigonometric functions. Section 4 illustrates validation studies and numerical results discussing effects of thickness stretching effect, length scale parameter, material composition, geometry parameters, and porosity level on natural frequency, and time history of poroelastic microplates. Conclusions are summarised in Section 5.

2. Mathematical formulations of poroelastic microplate

2.1. Material properties

Consider a poroelastic micro-size simply supported plate (with simply supported conditions at the edges) of width b, length a, and thickness h (Fig. 1). We assume an inhomogeneous microplate with continuous variation in their constituents and even distribution of porosity through the thickness. A modified micromechanical model is used to estimate the effective mechanical properties (density ρ, and Young's modulus E) as [39]

$$E(z) = \left[\left(E_c - E_m\right)\left(\frac{z}{h}+\frac{1}{2}\right)^n + E_m\right](1-\psi_z), \tag{1}$$

$$\rho(z) = \left[\left(\rho_c - \rho_m\right)\left(\frac{z}{h}+\frac{1}{2}\right)^n + \rho_m\right](1-\psi_z), \tag{2}$$

where c and m represent the ceramic and metal phases, n denotes the degree of continuous variation through-thickness, and ψ_z is a function for porosity distribution that in the current study a cosine function is used as [59]

$$\psi_z = \phi\cos\left[\pi\left(\frac{z}{h}\right)\right], \tag{3}$$

in which ϕ is porosity magnitude. Fig. 2 shows the variation of Young's modulus versus power law index.

2.2. Kinematics via a quasi-3D model in the MCS theory framework

This section develops a quasi-3D theory in the framework of the MCS theory for a poroelastic microplate. The displacement field is [60]

Table 4
Dimensionless natural frequencies of poroelastic microplates versus length-to-thickness ratio and material length-scale parameter, ($h = 17.6$ μm, $b/a = 1$, $n = 1$, ϕ=0.5).

	$\ell/h = 0.1$		$\ell/h = 0.2$		$\ell/h = 0.3$		$\ell/h = 0.5$	
a/*h*	CPT ($\varepsilon_z = 0$)	$\varepsilon_z \neq 0$	CPT ($\varepsilon_z = 0$)	$\varepsilon_z \neq 0$	CPT ($\varepsilon_z = 0$)	$\varepsilon_z \neq 0$	CPT ($\varepsilon_z = 0$)	$\varepsilon_z \neq 0$
(*m*,*n*)=(1,1)								
4	4.4008	3.9678	4.6698	4.2510	5.0864	4.6828	6.2330	5.8440
10	4.6575	4.6194	4.9429	4.9030	5.3850	5.3420	6.6036	6.5504
20	4.6975	4.7511	4.9853	5.0348	5.4312	5.4749	6.6604	6.6912
50	4.7088	4.7906	4.9973	5.0743	5.4443	5.5148	6.6765	6.7333
100	4.7104	4.7964	4.9991	5.0801	5.4462	5.5206	6.6788	6.7394
(*m*,*n*)=(1,2)								
4	10.0560	8.3233	10.6649	9.0359	11.6046	10.0976	14.1628	12.8605
10	11.4506	10.9821	12.1519	11.6908	13.2384	12.7826	16.2328	15.7661
20	11.6935	11.7086	12.4099	12.4178	13.5199	13.5167	16.5798	16.5475
50	11.7639	11.9480	12.4847	12.6572	13.6014	13.7582	16.6798	16.8028
100	11.7741	11.9838	12.4955	12.6930	13.6131	13.7942	16.6942	16.8409
(*m*,*n*)=(2,2)								
4	14.8786	11.8041	15.7662	12.9586	17.1282	14.6447	19.9089	18.9191
10	18.0248	16.8128	19.1282	17.9462	20.8373	19.6844	25.5456	24.4031
20	18.6301	18.4775	19.7716	19.6122	21.5399	21.3681	26.4145	26.2017
50	18.8093	19.0714	19.9618	20.2062	21.7473	21.9674	26.6693	26.8363
100	18.8352	19.1625	19.9893	20.2973	21.7773	22.0592	26.7061	26.932

$$\begin{Bmatrix} u_1 \\ u_2 \\ u_3 \end{Bmatrix} = \begin{Bmatrix} u(x,y) - z\dfrac{\partial w(x,y)}{\partial x} + f(z)\psi_1(x,y) \\ v(x,y) - z\dfrac{\partial w(x,y)}{\partial y} + f(z)\psi_2(x,y) \\ w(x,y) + f'(z)\psi_3(x,y) \end{Bmatrix}, \tag{4}$$

in which u_i: $i = 1,2,3$ denote the displacements in x-, y-, and z-directions, u, v, and w are mid-plane displacements, ψ_1, ψ_2, ψ_3 are rotations of normal to the mid-plane about y-axis, x-axis, and z-axis, respectively. $f(z)=z(1\text{-}4/3(z/h)^2)$ is the thickness function which represents related to the shear distribution along the thickness. In academic literature, the analysis of composite plates has primarily disregarded the influence of thickness stretching. However, many researchers, (e.g., Zenkour [61], Matsunaga [62] and Carrera et al. [63]) have explored the effect of thickness stretching in composite plates. This present study focuses on investigating the quasi-3D free and forced vibrations of poroelastic microsystem plates within the framework of the MCS theory.

According to the assumed displacement field in Eq. (4), the general strain displacement equations are [60]

$$\begin{aligned} \varepsilon_{xx} &= \frac{\partial u_1}{\partial x} = \frac{\partial u}{\partial x} - z\frac{\partial^2 w}{\partial x^2} + f(z)\frac{\partial \psi_1}{\partial x}, \\ \varepsilon_{yy} &= \frac{\partial u_2}{\partial y} = \frac{\partial v}{\partial y} - z\frac{\partial^2 w}{\partial y^2} + f(z)\frac{\partial \psi_2}{\partial y}, \\ \varepsilon_{zz} &= \frac{\partial u_3}{\partial z} = f''(z)\psi_3, \\ \gamma_{yz} &= \frac{\partial u_3}{\partial y} + \frac{\partial u_2}{\partial z} = f'(z)(\psi_2 + \frac{\partial \psi_3}{\partial y}), \\ \gamma_{xz} &= \frac{\partial u_3}{\partial x} + \frac{\partial u_1}{\partial z} = f'(z)(\psi_1 + \frac{\partial \psi_3}{\partial x}), \\ \gamma_{xy} &= \frac{\partial u_1}{\partial y} + \frac{\partial u_2}{\partial x} = \frac{\partial u}{\partial y} + \frac{\partial v}{\partial x} - 2z\frac{\partial^2 w}{\partial x \partial y} + f(z)(\frac{\partial \psi_2}{\partial x} + \frac{\partial \psi_1}{\partial y}). \end{aligned} \tag{5}$$

The kinetic energy in variational form of the poroelastic microplate is given by

$$\delta T = \frac{1}{2}\int_V (\dot{u}_i \delta \dot{u}_i)\mathrm{dV}, (i = 1,2,3), \tag{6}$$

where dV is an infinitesimal volume. The strain energy in a variational form for a poroelastic microplate is expressed by the MCS theory as [64]

$$\delta U = \int_V (\boldsymbol{m} : \delta\boldsymbol{\chi} + \boldsymbol{\sigma} : \delta\boldsymbol{\varepsilon})\mathrm{dV}, \tag{7}$$

in which $\{\mathbf{m}, \boldsymbol{\chi}, \boldsymbol{\sigma}, \boldsymbol{\varepsilon}\}$ are the deviatoric part of the symmetric couple stress tensor, the symmetric curvature tensor, the stress tensor, the strain tensor. The symmetric curvature tensor $\boldsymbol{\chi}$ is [65]

$$\boldsymbol{\chi} = \frac{1}{2}(\nabla\boldsymbol{\theta} + (\nabla\boldsymbol{\theta})^{\mathrm{T}}), \tag{8}$$

in which

$$\boldsymbol{\theta} = \frac{1}{2}curl(\boldsymbol{u}) = \begin{Bmatrix} \frac{1}{2}(\frac{\partial u_3}{\partial y} - \frac{\partial u_2}{\partial z}) \\ \frac{1}{2}(\frac{\partial u_1}{\partial z} - \frac{\partial u_3}{\partial x}) \\ \frac{1}{2}(\frac{\partial u_2}{\partial x} - \frac{\partial u_1}{\partial y}) \end{Bmatrix}. \tag{9}$$

Utilising Eq. (4) together with Eqs. (8) and (9) yields the components of the symmetric curvature tensor as

$$\begin{aligned} \chi_{xx} &= \frac{\partial^2 w}{\partial x \partial y} + \frac{1}{2}f'(z)(\frac{\partial^2 \psi_3}{\partial x \partial y} - \frac{\partial \psi_2}{\partial x}), \\ \chi_{yy} &= -\frac{\partial^2 w}{\partial x \partial y} + \frac{1}{2}f'(z)(\frac{\partial \psi_1}{\partial y} - \frac{\partial^2 \psi_3}{\partial x \partial y}), \\ \chi_{zz} &= \frac{1}{2}f'(z)(\frac{\partial \psi_2}{\partial x} - \frac{\partial \psi_1}{\partial y}), \\ \chi_{yz} &= \frac{1}{2}\left\{\frac{1}{2}f''(z)(\psi_1 - \frac{\partial \psi_3}{\partial x}) + \frac{1}{2}(\frac{\partial^2 v}{\partial x \partial y} - \frac{\partial^2 u}{\partial y^2} + f(z)(\frac{\partial^2 \psi_2}{\partial x \partial y} - \frac{\partial^2 \psi_1}{\partial y^2}))\right\}, \\ \chi_{xz} &= \frac{1}{2}\left\{\frac{1}{2}f''(z)(\frac{\partial \psi_3}{\partial y} - \psi_2) + \frac{1}{2}(\frac{\partial^2 v}{\partial x^2} - \frac{\partial^2 u}{\partial x \partial y} + f(z)(\frac{\partial^2 \psi_2}{\partial x^2} - \frac{\partial^2 \psi_1}{\partial x \partial y}))\right\}, \\ \chi_{xy} &= \frac{1}{2}\left\{\frac{\partial^2 w}{\partial y^2} + \frac{1}{2}f'(z)(\frac{\partial^2 \psi_3}{\partial y^2} - \frac{\partial \psi_2}{\partial y} + \frac{\partial \psi_1}{\partial x} - \frac{\partial^2 \psi_3}{\partial x^2}) - \frac{\partial^2 w}{\partial x^2}\right\}. \end{aligned} \tag{10}$$

The fundamental relations about an isotropic system can be

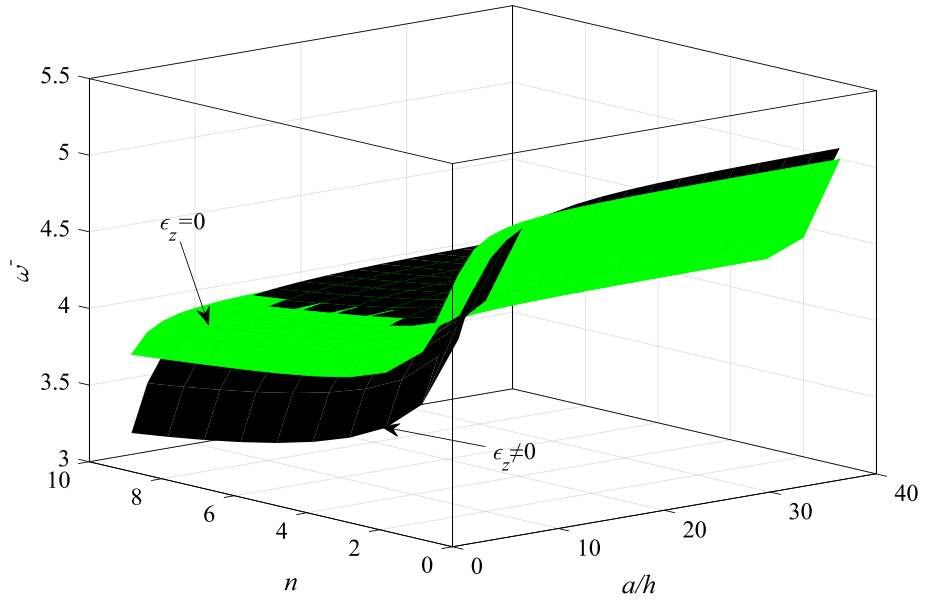

Fig. 3. Dimensionless fundamental frequency of poroelastic microplate against the material gradation constant and length-to-thickness ratio ($h = 17.6$ μm, $\ell/h = 0.2$, $b/a = 1$, ϕ=0.5).

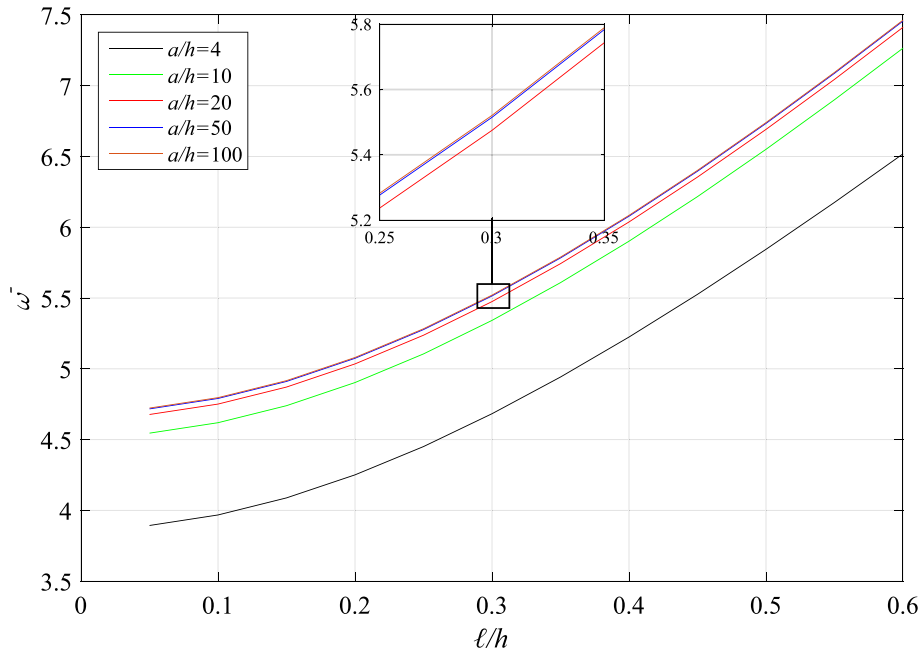

Fig. 4. Dimensionless fundamental frequency of poroelastic microplate versus different length-scale parameters for different length-to-thickness ratios ($h = 17.6$ μm, $b/a = 1$, $n = 1$, ϕ=0.5).

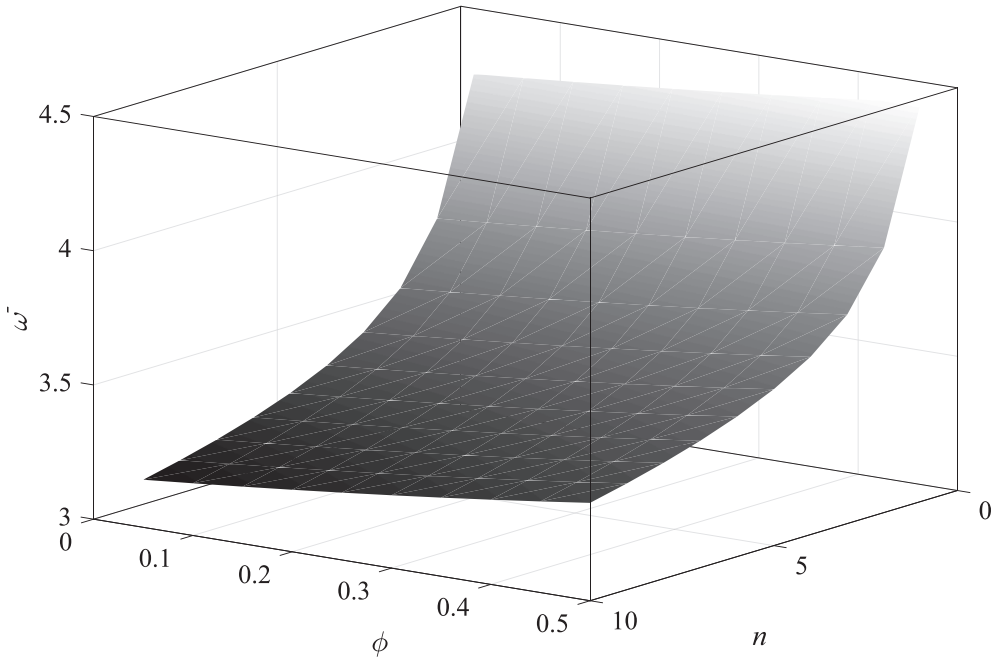

Fig. 5. Dimensionless fundamental frequency of poroelastic microplate against material composition and imperfections ($h = 17.6$ μm, $a/h = 5$, $b/a = 1$, $\ell/h = 0.2$).

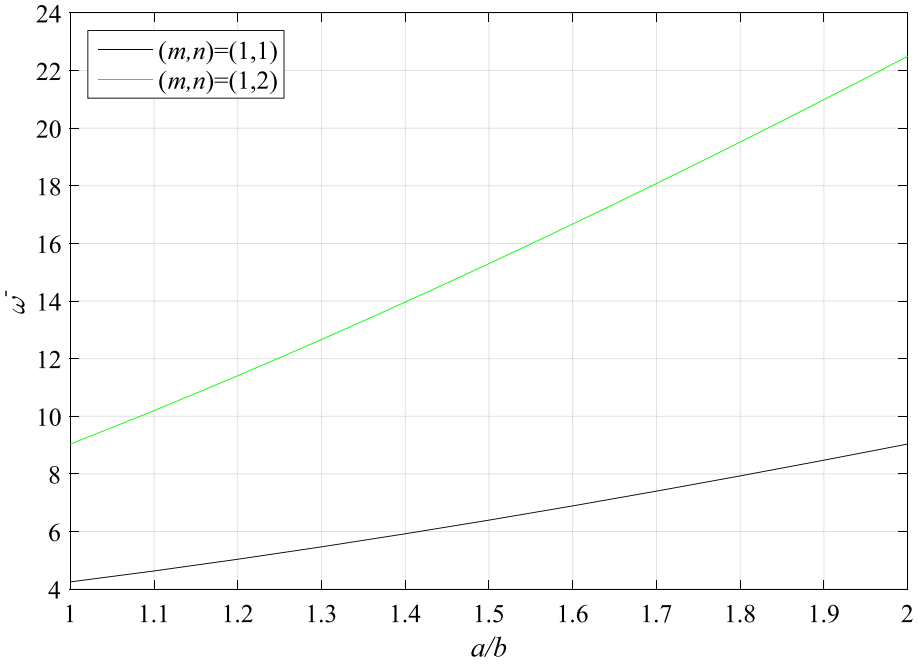

Fig. 6. Dimensionless natural frequencies of poroelastic microplate for (1,1) and (1,2) vibration modes versus width-to-length ratio ($h = 17.6$ μm, $a/h = 4$, $\ell/h = 0.2$, $n = 1$, ϕ=0.5).

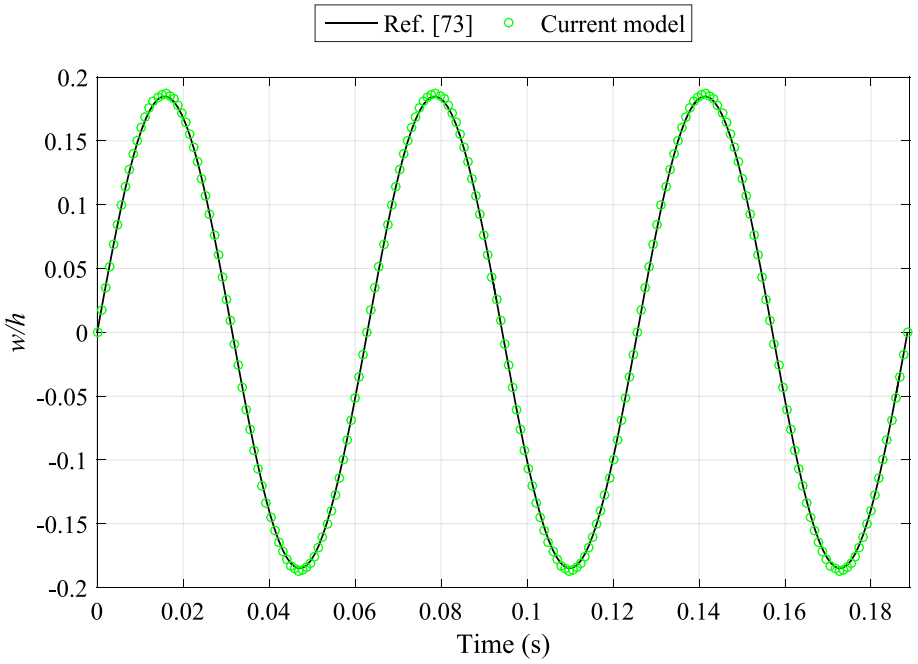

Fig. 7. Time history comparison of a square *macro*plate ($b/a = 1$, $a/h = 20$, $E = 71$ GPa, $\rho = 2699$ kg/m^3, $\nu = 0.34$, $\Omega = 100$ rad·s^{-1}).

(a)

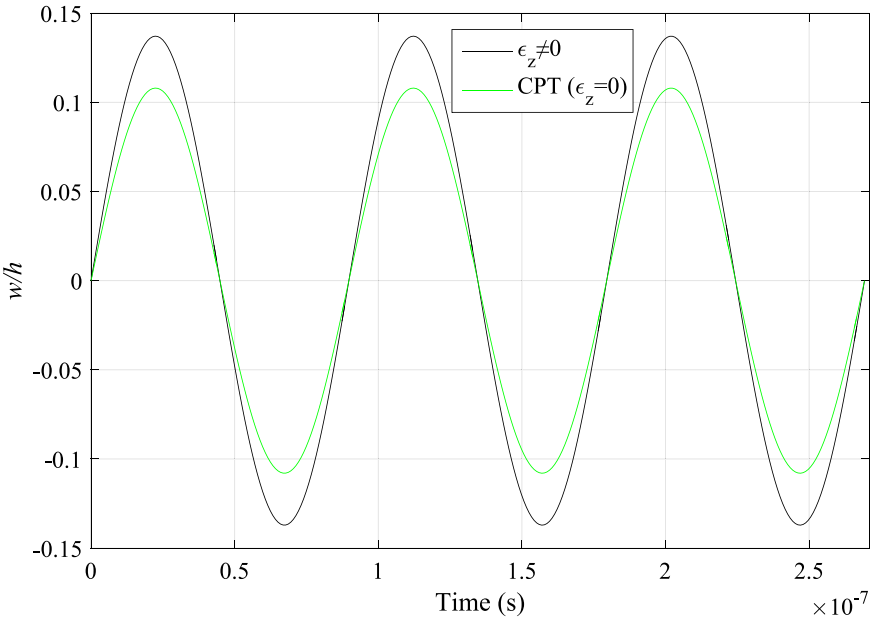

(b)

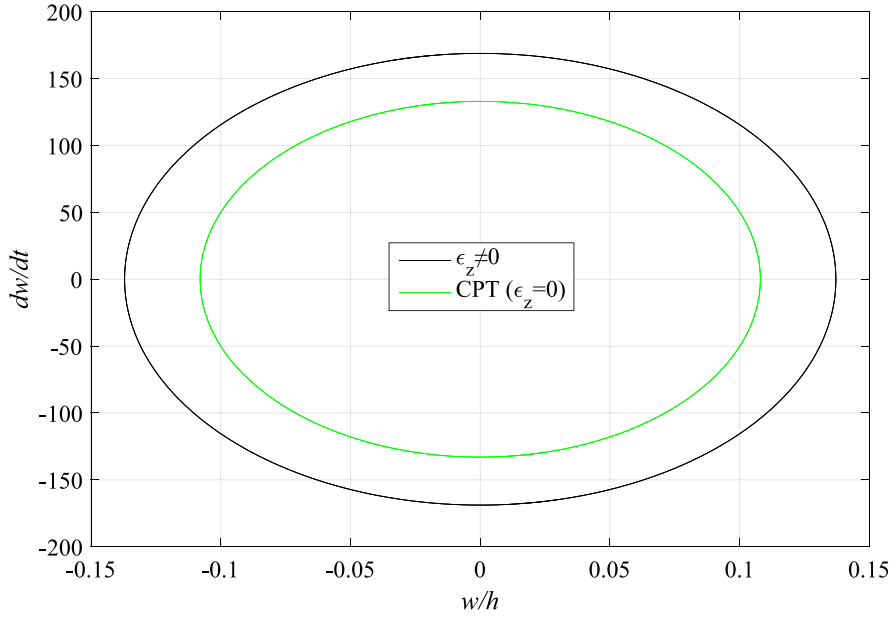

Fig. 8. Time history (a), and phase plot (b) diagram of poroelastic microplate (h = 17.6 μm, a/h = 4, b/a = 1, ℓ/h = 0.2, Ω = 7*1e^{7} rad·s^{-1}, n = 1, ϕ=0.5).

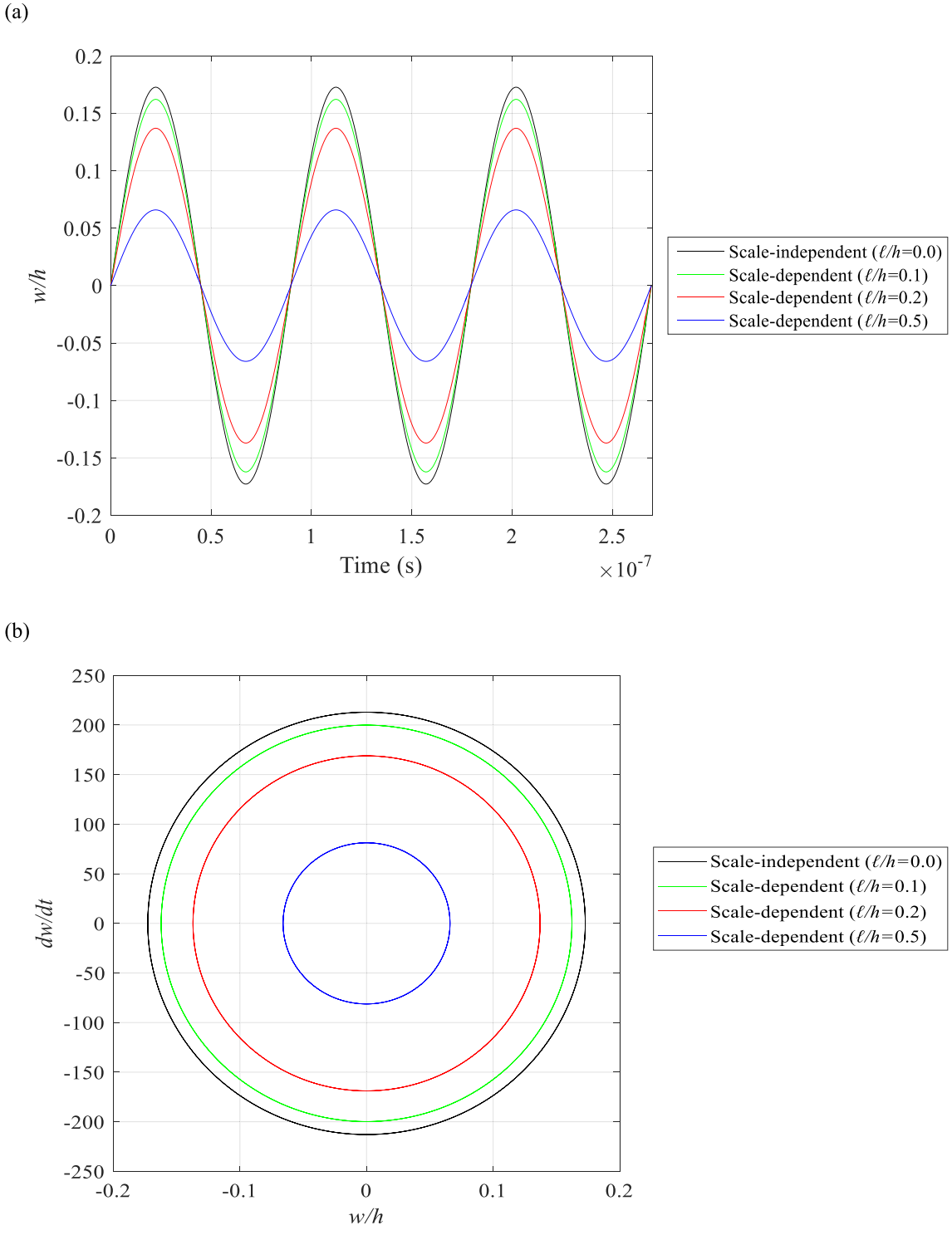

Fig. 9. Time history (a), and phase plot (b) diagram of poroelastic microplate versus size-dependence, (h = 17.6 μm, a/h = 4, b/a = 1, Ω = 7*1e^7 rad·s^{-1}, n = 1, ϕ=0.5).

(a)

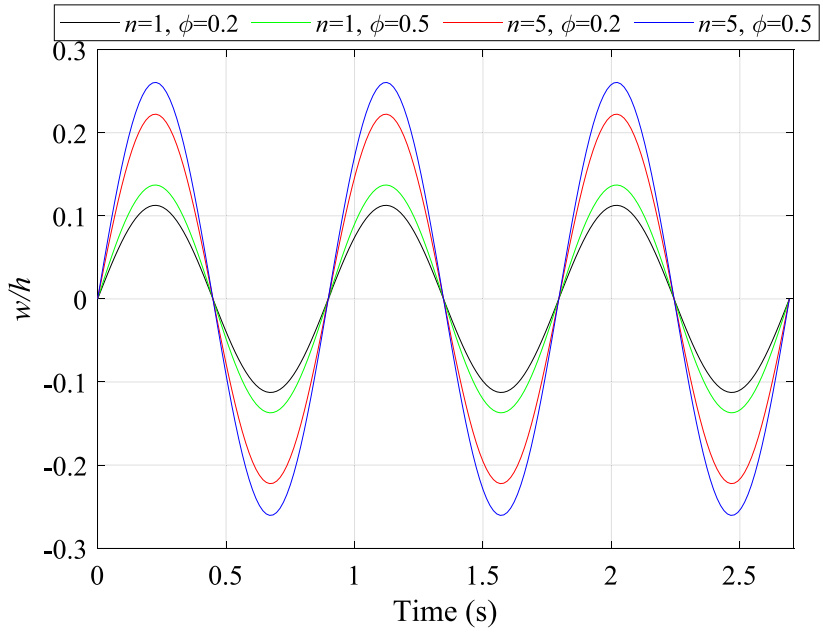

(b)

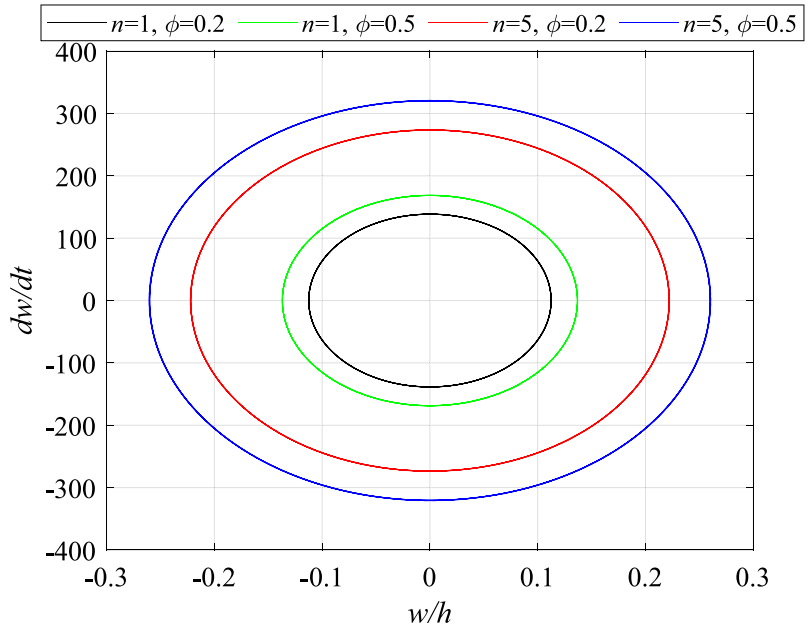

Fig. 10. Time history (a), and phase plot (b) diagram of poroelastic microplate against material composition and imperfections ($h = 17.6$ μm, $a/h = 4$, $b/a = 1$, $\ell/h = 0.2$, $\Omega = 7{*}1e^{7}$ rad·s^{-1}).

formulated by [66]

$$\sigma_{ij} = \lambda\delta_{ij}\varepsilon_{kk} + 2\mu\varepsilon_{ij}, \tag{11}$$

$$m_{ij} = 2\mu\ell^2\chi_{ij}, \tag{12}$$

where μ and λ denote the Lamé constants, and ℓ is the material length-scale parameter. For the poroelastic microplate, Eq. (11) reduces to

$$\begin{aligned}
\sigma_{xx} &= Q_{11}\left\{\frac{\partial u}{\partial x} - z\frac{\partial^2 w}{\partial x^2} + f(z)\frac{\partial\psi_1}{\partial x}\right\} + Q_{12}\left\{\frac{\partial v}{\partial y} - z\frac{\partial^2 w}{\partial y^2} + f(z)\frac{\partial\psi_2}{\partial y}\right\} + Q_{13}\{f''(z)\psi_3\},\\
\sigma_{yy} &= Q_{21}\left\{\frac{\partial u}{\partial x} - z\frac{\partial^2 w}{\partial x^2} + f(z)\frac{\partial\psi_1}{\partial x}\right\} + Q_{22}\left\{\frac{\partial v}{\partial y} - z\frac{\partial^2 w}{\partial y^2} + f(z)\frac{\partial\psi_2}{\partial y}\right\} + Q_{23}\{f''(z)\psi_3\},\\
\sigma_{zz} &= Q_{31}\left\{\frac{\partial u}{\partial x} - z\frac{\partial^2 w}{\partial x^2} + f(z)\frac{\partial\psi_1}{\partial x}\right\} + Q_{32}\left\{\frac{\partial v}{\partial y} - z\frac{\partial^2 w}{\partial y^2} + f(z)\frac{\partial\psi_2}{\partial y}\right\} + Q_{33}\{f''(z)\psi_3\},\\
\tau_{yz} &= Q_{44}\left\{f'(z)(\psi_2 + \frac{\partial\psi_3}{\partial y})\right\},\\
\tau_{xz} &= Q_{55}\left\{f'(z)(\psi_1 + \frac{\partial\psi_3}{\partial x})\right\},\\
\tau_{xy} &= Q_{66}\left\{\frac{\partial u}{\partial y} + \frac{\partial v}{\partial x} - 2z\frac{\partial^2 w}{\partial x\partial y} + f(z)(\frac{\partial\psi_2}{\partial x} + \frac{\partial\psi_1}{\partial y})\right\},
\end{aligned} \tag{13}$$

in which

$$\begin{aligned}
Q_{11} = Q_{22} = Q_{33} &= \frac{1-\nu}{\nu}\frac{\nu E(z)}{(1-2\nu)(1+\nu)},\\
Q_{12} = Q_{21} = Q_{13} = Q_{31} = Q_{23} = Q_{32} &= \frac{\nu E(z)}{(1-2\nu)(1+\nu)},\\
Q_{44} = Q_{55} = Q_{66} &= \frac{E(z)}{2+2\nu}.
\end{aligned} \tag{14}$$

By inserting Eq. (10) into Eq. (12), we have

$$\begin{aligned}
m_{xx} &= \frac{E(z)\ell^2}{1+\nu}\left\{\frac{\partial^2 w}{\partial x\partial y} + \frac{1}{2}f'(z)(\frac{\partial^2\psi_3}{\partial x\partial y} - \frac{\partial\psi_2}{\partial x})\right\},\\
m_{yy} &= \frac{E(z)\ell^2}{1+\nu}\left\{-\frac{\partial^2 w}{\partial x\partial y} + \frac{1}{2}f'(z)(\frac{\partial\psi_1}{\partial y} - \frac{\partial^2\psi_3}{\partial x\partial y})\right\},\\
m_{zz} &= \frac{E(z)\ell^2}{1+\nu}\left\{\frac{1}{2}f'(z)(\frac{\partial\psi_2}{\partial x} - \frac{\partial\psi_1}{\partial y})\right\},\\
m_{yz} &= \frac{E(z)\ell^2}{2+2\nu}\left\{\frac{1}{2}f''(z)(\psi_1 - \frac{\partial\psi_3}{\partial x}) + \frac{1}{2}(\frac{\partial^2 v}{\partial x\partial y} - \frac{\partial^2 u}{\partial y^2} + f(z)(\frac{\partial^2\psi_2}{\partial x\partial y} - \frac{\partial^2\psi_1}{\partial y^2}))\right\},\\
m_{xz} &= \frac{E(z)\ell^2}{2+2\nu}\left\{\frac{1}{2}f''(z)(\frac{\partial\psi_3}{\partial y} - \psi_2) + \frac{1}{2}(\frac{\partial^2 v}{\partial x^2} - \frac{\partial^2 u}{\partial x\partial y} + f(z)(\frac{\partial^2\psi_2}{\partial x^2} - \frac{\partial^2\psi_1}{\partial x\partial y}))\right\},\\
m_{xy} &= \frac{E(z)\ell^2}{2+2\nu}\left\{\frac{\partial^2 w}{\partial y^2} + \frac{1}{2}f'(z)(\frac{\partial^2\psi_3}{\partial y^2} - \frac{\partial\psi_2}{\partial y} + \frac{\partial\psi_1}{\partial x} - \frac{\partial^2\psi_3}{\partial x^2}) - \frac{\partial^2 w}{\partial x^2}\right\}.
\end{aligned} \tag{15}$$

Using Eqs. (5), (10), (13), and (15) and inserting them into the potential energy (Eq. (7)), the strain energy of a poroelastic quasi-3D microplate via the MCS theory is given by

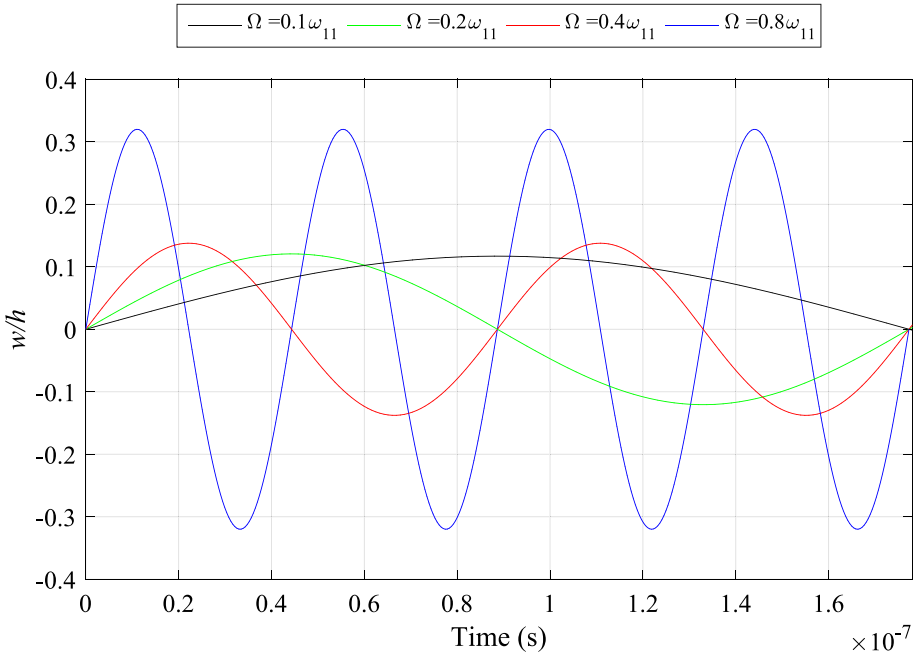

Fig. 11. Time history of poroelastic microplate versus excitation frequency (h = 17.6 μm, a/h = 4, b/a = 1, ℓ/h = 0.2, n = 1, ϕ=0.5).

$$\delta U=\int_V\Big\{\sigma_{xx}(\frac{\partial\delta u}{\partial x}-z\frac{\partial^2\delta w}{\partial x^2}+f(z)\frac{\partial\delta\psi_1}{\partial x})+\sigma_{yy}(\frac{\partial\delta v}{\partial y}-z\frac{\partial^2\delta w}{\partial y^2}+f(z)\frac{\partial\delta\psi_2}{\partial y})$$
$$+\sigma_{zz}(f^{''}(z)\delta\psi_3)+\tau_{yz}(f^{'}(z)(\delta\psi_2+\frac{\partial\delta\psi_3}{\partial y}))+\tau_{xz}(f^{'}(z)(\delta\psi_1+\frac{\partial\delta\psi_3}{\partial x}))$$
$$+\tau_{xy}(\frac{\partial\delta u}{\partial y}+\frac{\partial\delta v}{\partial x}-2z\frac{\partial^2\delta w}{\partial x\partial y}+f(z)(\frac{\partial\delta\psi_2}{\partial x}+\frac{\partial\delta\psi_1}{\partial y}))\Big\}\mathrm{dV}$$
$$+\int_V\Big\{m_{xx}(\frac{\partial^2\delta w}{\partial x\partial y}+\frac{1}{2}f^{'}(z)(\frac{\partial^2\delta\psi_3}{\partial x\partial y}-\frac{\partial\delta\psi_2}{\partial x}))+m_{yy}(-\frac{\partial^2\delta w}{\partial x\partial y}+\frac{1}{2}f^{'}(z)(\frac{\partial\delta\psi_1}{\partial y}-\frac{\partial^2\delta\psi_3}{\partial x\partial y}))$$
$$+m_{zz}(\frac{1}{2}f^{'}(z)(\frac{\partial\delta\psi_2}{\partial x}-\frac{\partial\delta\psi_1}{\partial y}))$$
$$+2m_{yz}(\Big\{\frac{1}{4}f^{''}(z)(\delta\psi_1-\frac{\partial\delta\psi_3}{\partial x})+\frac{1}{4}(\frac{\partial^2\delta v}{\partial x\partial y}-\frac{\partial^2\delta u}{\partial y^2}+f(z)(\frac{\partial^2\delta\psi_2}{\partial x\partial y}-\frac{\partial^2\delta\psi_1}{\partial y^2}))\Big\}\Big)$$
$$+2m_{xz}(\Big\{\frac{1}{4}f^{''}(z)(\frac{\partial\delta\psi_3}{\partial y}-\delta\psi_2)+\frac{1}{4}(\frac{\partial^2\delta v}{\partial x^2}-\frac{\partial^2\delta u}{\partial x\partial y}+f(z)(\frac{\partial^2\delta\psi_2}{\partial x^2}-\frac{\partial^2\delta\psi_1}{\partial x\partial y}))\Big\}\Big)$$
$$+2m_{xy}(\frac{1}{2}\Big\{\frac{\partial^2\delta w}{\partial y^2}+\frac{1}{2}f^{'}(z)(\frac{\partial^2\delta\psi_3}{\partial y^2}-\frac{\partial\delta\psi_2}{\partial y}+\frac{\partial\delta\psi_1}{\partial x}-\frac{\partial^2\delta\psi_3}{\partial x^2})-\frac{\partial^2\delta w}{\partial x^2}\Big\}\Big)\Big\}\mathrm{dV}. \tag{16}$$

Considering an external mechanical load, the virtual work can be formulated as

$$\delta W=-\int_A q\delta u_3\mathrm{dA}. \tag{17}$$

Using the Hamilton's Principle

$$\int_{t_1}^{t_2}(\delta U-\delta T+\delta W)dt=0, \tag{18}$$

yields to the following

$$\frac{\partial N_{xx}}{\partial x}+\frac{\partial N_{xy}}{\partial y}+\frac{1}{2}\frac{\partial^2 R_{xz}}{\partial x\partial y}+\frac{1}{2}\frac{\partial^2 R_{yz}}{\partial y^2}=I_1\frac{\partial^2 u}{\partial t^2}-I_2\frac{\partial^3 w}{\partial x\partial t^2}+I_4\frac{\partial^2\psi_1}{\partial t^2}, \tag{19}$$

$$\frac{\partial N_{xy}}{\partial x}+\frac{\partial N_{yy}}{\partial y}-\frac{1}{2}\frac{\partial^2 R_{xz}}{\partial x^2}-\frac{1}{2}\frac{\partial^2 R_{yz}}{\partial x\partial y}=I_1\frac{\partial^2 v}{\partial t^2}-I_2\frac{\partial^3 w}{\partial y\partial t^2}+I_4\frac{\partial^2\psi_2}{\partial t^2}, \tag{20}$$

$$\frac{\partial^2 M_{xx}}{\partial x^2}+\frac{\partial^2 M_{yy}}{\partial y^2}+2\frac{\partial^2 M_{xy}}{\partial x\partial y}-\frac{\partial^2 R_{xx}}{\partial x\partial y}+\frac{\partial^2 R_{yy}}{\partial x\partial y}-\frac{\partial^2 R_{xy}}{\partial y^2}+\frac{\partial^2 R_{xy}}{\partial x^2}-q$$
$$=I_1\frac{\partial^2 w}{\partial t^2}+I_2(\frac{\partial^3 u}{\partial x\partial t^2}+\frac{\partial^3 v}{\partial y\partial t^2})-I_3(\frac{\partial^4 w}{\partial x^2\partial t^2}+\frac{\partial^4 w}{\partial y^2\partial t^2})+I_5(\frac{\partial^3\psi_1}{\partial x\partial t^2}+\frac{\partial^3\psi_2}{\partial y\partial t^2})+I_7\frac{\partial^2\psi_3}{\partial t^2}, \tag{21}$$

$$\frac{\partial O_{xx}}{\partial x}+\frac{\partial O_{xy}}{\partial y}-P_{xz}+\frac{1}{2}\frac{\partial S_{yy}}{\partial y}-\frac{1}{2}\frac{\partial S_{zz}}{\partial y}+\frac{1}{2}\frac{\partial S_{xy}}{\partial x}+\frac{1}{2}\frac{\partial^2 T_{xz}}{\partial x\partial y}+\frac{1}{2}\frac{\partial^2 T_{yz}}{\partial y^2}-\frac{1}{2}U_{yz}$$
$$=I_4\frac{\partial^2 u}{\partial t^2}-I_5\frac{\partial^3 w}{\partial x\partial t^2}+I_6\frac{\partial^2\psi_1}{\partial t^2}, \tag{22}$$

$$\frac{\partial O_{xy}}{\partial x}+\frac{\partial O_{yy}}{\partial y}-P_{yz}-\frac{1}{2}\frac{\partial S_{xx}}{\partial x}+\frac{1}{2}\frac{\partial S_{zz}}{\partial x}-\frac{1}{2}\frac{\partial S_{xy}}{\partial y}-\frac{1}{2}\frac{\partial^2 T_{xz}}{\partial x^2}-\frac{1}{2}\frac{\partial^2 T_{yz}}{\partial x\partial y}+\frac{1}{2}U_{xz}$$
$$=I_4\frac{\partial^2 v}{\partial t^2}-I_5\frac{\partial^3 w}{\partial y\partial t^2}+I_6\frac{\partial^2\psi_2}{\partial t^2}, \tag{23}$$

$$-L_{zz}+\frac{\partial P_{xz}}{\partial x}+\frac{\partial P_{yz}}{\partial y}-\frac{1}{2}\frac{\partial^2 S_{xx}}{\partial x\partial y}+\frac{1}{2}\frac{\partial^2 S_{yy}}{\partial x\partial y}-\frac{1}{2}\frac{\partial^2 S_{xy}}{\partial y^2}+\frac{1}{2}\frac{\partial^2 S_{xy}}{\partial x^2}+\frac{1}{2}\frac{\partial U_{xz}}{\partial y}-\frac{1}{2}\frac{\partial U_{yz}}{\partial x}$$
$$=I_7\frac{\partial^2 w}{\partial t^2}+I_8\frac{\partial^2\psi_3}{\partial t^2}, \tag{24}$$

in which

$$N_{ij}=\int_{-\frac{h}{2}}^{\frac{h}{2}}\sigma_{ij}dz,$$
$$M_{ij}=\int_{-\frac{h}{2}}^{\frac{h}{2}}z\sigma_{ij}dz,$$
$$O_{ij}=\int_{-\frac{h}{2}}^{\frac{h}{2}}f(z)\sigma_{ij}dz,$$
$$P_{ij}=\int_{-\frac{h}{2}}^{\frac{h}{2}}f^{'}(z)\sigma_{ij}dz,$$
$$L_{ij}=\int_{-\frac{h}{2}}^{\frac{h}{2}}f^{''}(z)\sigma_{ij}dz,$$
$$R_{ij}=\int_{-\frac{h}{2}}^{\frac{h}{2}}m_{ij}dz,$$
$$S_{ij}=\int_{-\frac{h}{2}}^{\frac{h}{2}}f^{'}(z)m_{ij}dz,$$
$$T_{ij}=\int_{-\frac{h}{2}}^{\frac{h}{2}}f(z)m_{ij}dz,$$
$$U_{ij}=\int_{-\frac{h}{2}}^{\frac{h}{2}}f^{''}(z)m_{ij}dz, \tag{25}$$

and

$$(I_1,I_2,I_3,I_4,I_5,I_6,I_7,I_8)$$
$$=\int_{-\frac{h}{2}}^{\frac{h}{2}}\rho(z)(1,z,z^2,f(z),zf(z),[f(z)]^2,f^{'}(z),[f^{'}(z)]^2)dz. \tag{26}$$

One may derive the governing motion equations in terms of displacement components by inserting Eqs. (13) and (15) into Eq. (25), and also inserting the resultants into Eqs. (19)-(24), which are presented in Appendix A.

3. Solution procedure

This paper uses a numerical technique that relies on trigonometric functions to assess vibration modes. The kinematic boundary condition for the poroelastic quasi-3D microplates is considered as simply supported at the edges.

3.1. Free vibration analysis

To approximate axial-transverse-rotation-stretching characteristics and satisfy the simply supported conditions at all edges of the microplate, the following series are used.

$$\begin{Bmatrix}u(x,y)\\v(x,y)\\w(x,y)\\\psi_1(x,y)\\\psi_2(x,y)\\\psi_3(x,y)\end{Bmatrix}=\sum_{m=1}^{\infty}\sum_{n=1}^{\infty}\begin{Bmatrix}U_{mn}\cos\frac{m\pi x}{a}\sin\frac{n\pi y}{b}\\V_{mn}\sin\frac{m\pi x}{a}\cos\frac{n\pi y}{b}\\W_{mn}\sin\frac{m\pi x}{a}\sin\frac{n\pi y}{b}\\\Psi^1_{mn}\cos\frac{m\pi x}{a}\sin\frac{n\pi y}{b}\\\Psi^2_{mn}\sin\frac{m\pi x}{a}\cos\frac{n\pi y}{b}\\\Psi^3_{mn}\sin\frac{m\pi x}{a}\sin\frac{n\pi y}{b}\end{Bmatrix}\exp(i\omega t), \tag{27}$$

in which ω denotes the natural frequency, denotes the associated amplitudes.

3.2. Forced vibration analysis

While satisfying the boundary conditions, the displacement components are described by the following expressions

$$\begin{Bmatrix} u(x,y) \\ v(x,y) \\ w(x,y) \\ \psi_1(x,y) \\ \psi_2(x,y) \\ \psi_3(x,y) \end{Bmatrix} = \sum_{m=1}^{\infty}\sum_{n=1}^{\infty} \begin{Bmatrix} U_{mn}\cos\frac{m\pi x}{a}\sin\frac{n\pi y}{b} \\ V_{mn}\sin\frac{m\pi x}{a}\cos\frac{n\pi y}{b} \\ W_{mn}\sin\frac{m\pi x}{a}\sin\frac{n\pi y}{b} \\ \Psi^1_{mn}\cos\frac{m\pi x}{a}\sin\frac{n\pi y}{b} \\ \Psi^2_{mn}\sin\frac{m\pi x}{a}\cos\frac{n\pi y}{b} \\ \Psi^3_{mn}\sin\frac{m\pi x}{a}\sin\frac{n\pi y}{b} \end{Bmatrix} \sin(\Omega t), \tag{28}$$

herein Ω represents the excitation frequency. The assumption is made that the load is distributed sinusoidally as a dynamic load, and it is represented by the following expression:

$$q = \sum_{m=1}^{\infty} Q_{mn}\sin\frac{m\pi x}{a}\sin\frac{n\pi y}{b}\sin(\Omega t), \tag{29}$$

in which Q_{mn} is associated with a sinusoidal distribution that is given by

$$Q_{mn} = q_0, \tag{30}$$

with q_0 is the intensity of the distributed load.

4. Results and discussions for free and forced vibrations

The free and forced vibrations of poroelastic micro-sized plates are studied. The microplate is made of FGMs (Al/SiC) with Young's moduli ($E_m = 71$ GPa, and $E_c = 427$ GPa), and mass density ($\rho_m = 2699$ kg/m^3, and $\rho_c = 3100$ kg/m^3). Poisson's ratio ν is taken as 0.30 along the thickness. For simplicity, this paper presents the results of free vibration in the following dimensionless form.

$$\overline{\omega}_{mn} = \omega_{mn}a^2/h\sqrt{\rho_c/E_c}. \tag{31}$$

4.1. Free vibration analysis

Study 1: Various numerical validations for a simpler version of the system.

As the first part of the study, the natural frequency of thin-elastic *macro*plate is analysed using the solution procedure outlined in Section 3 (ignoring length-scale parameter, being functionally graded as well as the porosity) and is evaluated through a comparative analysis with the results obtained from a finite element software. The plate is assumed to be fabricated of Aluminum (Al 99.9) with dimensions 0.10 × 0.10 × 0.001 m, and simply supported conditions at all the edges. The natural fundamental and (1,2), (2,1), (2,2), (1,3), (3,1), (2,3), (3,2), (1,4), and (4,1) frequencies are shown in Table 1. Comparison of the current findings with those obtained from ANSYS [67] shows a very good agreement between the results.

Table 2 tabulates the comparison of the dimensionless natural frequencies with those of Zhou et al. [68], Jha et al. [69], and Benahmed et al. [70] via 3D exact and quasi-3D theories for a square *macro*plate where the effects of length scale parameter, being functionally graded and material imperfection are cancelled. For all the data, good agreements can be observed.

Table 3 shows the dimensionless fundamental frequency for FGM square microplates without porosity imperfections. The present results are in very good agreement with those obtained by Thai et al. [71], and Jung et al. [72] via classical and higher-order shear deformable plate theories in the framework of the MCS theory.

Study 2: Influence of thickness stretching (via the quasi-3D poroelasticity) on the natural frequencies.

In Table 4, the effect of small-scale parameters and length-to-thickness ratio on the dimensionless natural frequencies of a simply supported poroelastic microplate is tabulated using a quasi-3D theory and also classical plate theory (CPT). For the natural frequencies, it can be seen that increasing the small-scale parameter increases the frequency of the system and this conclusion is independent of vibration modes. It also can be seen that including the thickness stretching affects the responses, especially those of thicker microplates.

To have an even further understanding of the stretching effect, the variations of the dimensionless fundamental frequency of the microplate have been plotted in Fig. 3 for both CPT and quasi-3D models when varying the material gradation constant and the length-to-thickness ratio.

Study 3: Influence of size-dependence on the natural frequencies.

Influence of the length scale parameter on the dimensionless fundamental frequency of the poroelastic microplate is plotted versus the length-to-thickness ratio in Fig. 4. As seen in this figure, an increase in the length scale parameter results in a higher dimensionless fundamental frequency for all the cases. Moreover, as the value of the length-to-thickness ratio increases, the difference in fundamental frequency between different cases becomes smaller.

Study 4: Influence of material composition and porosity imperfections on the natural frequencies.

Fig. 5 illustrates the variations in the dimensionless fundamental frequency versus the material composition representative (n) and porosity (voids) level (ϕ). It can be seen that, for this specific porosity distribution, an increase in the material imperfection level results in a notable change in the frequency. Furthermore, increasing the material gradation constant causes a prominent effect on microsystem's response, which aligns perfectly with the nature of the materials used.

Study 5: Influence of geometrical parameters on the natural frequencies.

Fig. 6 presents the influence of the length-to-width ratio of the poroelastic quasi-3D microplate on the dimensionless natural frequencies. Moreover, this effect is particularly significant for the (1,2) vibrational mode in comparison to the fundamental mode.

4.2. Forced vibration analysis

Study 1: Numerical validations with simpler models.

The time history, which refers to the time-dependent central deflection, of a *macro*size square plate (with no length-scale effects, not being functionally graded, without material imperfection) is obtained here. We compare and validate it against the results obtained for a Kirchhoff plate theory by Papargyri-Beskou and Beskos [73] and illustrated in Fig. 7, showing very good agreement.

Study 2: Influence of thickness stretching on time histories.

A comparison between the present quasi-3D model ($\varepsilon_z \neq 0$) and CPT ($\varepsilon_z = 0$) for time history and phase plot diagram of a thick micro-size plate is depicted in Fig. 8. From this figure, it has been observed that the thickness stretching has an important influence on the behaviour of the poroelastic microplate, especially for higher values of amplitude.

Study 3: Influence of size-dependence on time histories.

Fig. 9 illustrates the effect of size-dependence on the forced dynamic response of the poroelastic microplate. The results demonstrate that an increase in the small-scale length scale parameter leads to an elevation in body's stiffness, subsequently causing a reduction in the amplitude of vibrations. In other words, as the small-scale parameter grows, the phase

plot trajectory becomes smaller.

Study 4: Influence of material composition and porosity imperfections on time histories.

To illustrate the sensitivity of the forced vibration, Fig. 10 depicts the variation of transverse deflection over time for several material gradation constants and porosity levels. As seen, increasing the material gradation constant and porosity level leads to an increase in the amplitude.

Study 5: Influence of excitation frequency on time histories.

Effects of excitation frequency on the dynamic response of the quasi-3D microsystem are illustrated in Fig. 11. Increasing the excitation frequency results in an increment in both the amplitude value and the number of oscillations. In other words, as the excitation frequency approaches the resonant frequency, the transverse deflection becomes larger, and the oscillations occur at a faster rate.

5. Conclusions

In this paper, a quasi-3D model for poroelastic microplate structures was developed to study the free and forced vibrations. A combination of a higher-order quasi-3D shear deformable model, together with the MCS theory, was used to formulate the poroelastic microplate system. Using Hamilton's principle, the governing motion equations (in-plane and out-of-plane including stretching) were derived, which possess fourfold coupled (axial-transverse-rotation-stretching) characteristics. By using a numerical technique, a set of trigonometric functions was applied to solve the governing equations and the accuracy of the model was validated, showing very good accuracy. Effect of thickness stretching, material composition and imperfections, and length-scale parameters were studied on the natural frequency and time history perspectives. Based on the analysis of the parameters examined within the microsystem range, it was determined that: for the free vibration analysis, it was shown that, for the study cases, the thickness stretching, material composition and imperfections have important effects on the response of the microplate, especially for thick microplates; for example, considering the stretching effect (versus CPT) alter the natural frequencies. Moreover, it was observed that an increase in the small-scale length scale parameter of the poroelastic microstructure leads to an increase in the dimensionless fundamental natural frequency of the microplate. Additionally, a higher dimensionless fundamental frequency was achieved by increasing the length-to-thickness ratio.

The forced vibration analysis, on the other hand, demonstrated that by increasing the small-scale length scale parameter in the examined scenario, the amplitude of vibrations decreases, hence causing the phase plot trajectory to become smaller. Furthermore, for the considered material composition and porosity distribution model, increasing the power-law index and porosity level results in an increase in the amplitude. Moreover, as the excitation frequency approaches the resonant frequency, the transverse vibration amplitude increases, and the oscillations occur at a faster rate.

CRediT authorship contribution statement

Behrouz Karami: Conceptualization, Data curation, Formal analysis, Investigation, Methodology, Software, Validation, Writing – original draft. **Mergen H. Ghayesh:** Conceptualization, Formal analysis, Supervision, Writing – review & editing, Methodology. **Nicholas Fantuzzi:** Conceptualization, Formal analysis, Writing – review & editing.

Declaration of competing interest

The authors declare the following financial interests/personal relationships which may be considered as potential competing interests: Behrouz Karami reports was provided by The University of Adelaide. Nicholas Fantuzzi, Co Editors-in-Chief If there are other authors, they declare that they have no known competing financial interests or personal relationships that could have appeared to influence the work reported in this paper.

Data availability

Data will be made available on request.

Acknowledgements

The Higher Degree by Research support through the University of Adelaide, and Faculty of Sciences, Engineering and Technology, the University of Adelaide, is acknowledged.

Appendix A

$$
\begin{aligned}
&A_{11}\frac{\partial^2 u}{\partial x^2}-B_{11}\frac{\partial^3 w}{\partial x^3}+D_{11}\frac{\partial^2 \psi_1}{\partial x^2}+A_{12}\frac{\partial^2 v}{\partial x\partial y}-B_{12}\frac{\partial^3 w}{\partial x\partial y^2}+D_{12}\frac{\partial^2 \psi_2}{\partial x\partial y}\\
&+E_{13}\frac{\partial \psi_3}{\partial x}+A_{66}\left(\frac{\partial^2 u}{\partial y^2}+\frac{\partial^2 v}{\partial x\partial y}\right)-2B_{66}\frac{\partial^3 w}{\partial x\partial y^2}+D_{66}\left(\frac{\partial^2 \psi_2}{\partial x\partial y}+\frac{\partial^2 \psi_1}{\partial y^2}\right)\\
&+\frac{1}{4}\left\{A_{00}\left(\frac{\partial^4 v}{\partial x^3\partial y}-\frac{\partial^4 u}{\partial x^2\partial y^2}\right)+D_{00}\left(\frac{\partial^4 \psi_2}{\partial x^3\partial y}-\frac{\partial^4 \psi_1}{\partial x^2\partial y^2}\right)+E_{00}\left(\frac{\partial^3 \psi_3}{\partial x\partial y^2}-\frac{\partial^2 \psi_2}{\partial x\partial y}\right)\right\}\\
&+\frac{1}{4}\left\{A_{00}\left(\frac{\partial^4 v}{\partial x\partial y^3}-\frac{\partial^4 u}{\partial y^4}\right)+D_{00}\left(\frac{\partial^4 \psi_2}{\partial x\partial y^3}-\frac{\partial^4 \psi_1}{\partial y^4}\right)+E_{00}\left(\frac{\partial^2 \psi_1}{\partial y^2}-\frac{\partial^3 \psi_3}{\partial x\partial y^2}\right)\right\}\\
&=I_1\frac{\partial^2 u}{\partial t^2}-I_2\frac{\partial^3 w}{\partial x\partial t^2}+I_4\frac{\partial^2 \psi_1}{\partial t^2},
\end{aligned}
\tag{A1}
$$

$$
\begin{aligned}
&A_{66}(\frac{\partial^2 u}{\partial x\partial y}+\frac{\partial^2 v}{\partial x^2})-2B_{66}\frac{\partial^3 w}{\partial x^2\partial y}+D_{66}(\frac{\partial^2 \psi_2}{\partial x^2}+\frac{\partial^2 \psi_1}{\partial x\partial y})+A_{21}\frac{\partial^2 u}{\partial y\partial x}\\
&-B_{21}\frac{\partial^3 w}{\partial x^2\partial y}+D_{21}\frac{\partial^2 \psi_1}{\partial x\partial y}+A_{22}\frac{\partial^2 v}{\partial y^2}-B_{22}\frac{\partial^3 w}{\partial y^3}+D_{22}\frac{\partial^2 \psi_2}{\partial y^2}+E_{23}\frac{\partial \psi_3}{\partial y}\\
&-\frac{1}{4}\left\{A_{00}(\frac{\partial^4 v}{\partial x^4}-\frac{\partial^4 u}{\partial x^3\partial y})+D_{00}(\frac{\partial^4 \psi_2}{\partial x^4}-\frac{\partial^4 \psi_1}{\partial x^3\partial y})+E_{00}(\frac{\partial^3 \psi_3}{\partial x^2\partial y}-\frac{\partial^2 \psi_2}{\partial x^2})\right\}\\
&-\frac{1}{4}\left\{A_{00}(\frac{\partial^4 v}{\partial x^2\partial y^2}-\frac{\partial^4 u}{\partial x\partial y^3})+D_{00}(\frac{\partial^4 \psi_2}{\partial x^2\partial y^2}-\frac{\partial^4 \psi_1}{\partial x\partial y^3})+E_{00}(\frac{\partial^2 \psi_1}{\partial x\partial y}-\frac{\partial^3 \psi_3}{\partial x^2\partial y})\right\}\\
&=I_1\frac{\partial^2 v}{\partial t^2}-I_2\frac{\partial^3 w}{\partial y\partial t^2}+I_4\frac{\partial^2 \psi_2}{\partial t^2},
\end{aligned}
\tag{A2}
$$

$$
\begin{aligned}
&B_{11}\frac{\partial^3 u}{\partial x^3}-F_{11}\frac{\partial^4 w}{\partial x^4}+G_{11}\frac{\partial^3 \psi_1}{\partial x^3}+B_{12}\frac{\partial^2 v}{\partial x^2\partial y}-F_{12}\frac{\partial^4 w}{\partial x^2\partial y^2}+G_{12}\frac{\partial^3 \psi_2}{\partial x^2\partial y}+H_{13}\frac{\partial^2 \psi_3}{\partial x^2}\\
&+B_{21}\frac{\partial^3 u}{\partial x\partial y^2}-F_{21}\frac{\partial^4 w}{\partial x^2\partial y^2}+G_{21}\frac{\partial^3 \psi_1}{\partial x\partial y^2}+B_{22}\frac{\partial^3 v}{\partial y^3}-F_{22}\frac{\partial^4 w}{\partial y^4}+G_{22}\frac{\partial^3 \psi_2}{\partial y^3}+H_{23}\frac{\partial^2 \psi_3}{\partial y^2}\\
&+2B_{66}(\frac{\partial^3 u}{\partial x\partial y^2}+\frac{\partial^3 v}{\partial x^2\partial y})-4F_{66}\frac{\partial^4 w}{\partial x^2\partial y^2}+2G_{66}(\frac{\partial^3 \psi_2}{\partial x^2\partial y}+\frac{\partial^3 \psi_1}{\partial x\partial y^2})\\
&-2A_{00}\frac{\partial^4 w}{\partial x^2\partial y^2}-J_{00}(\frac{\partial^4 \psi_3}{\partial x^2\partial y^2}-\frac{\partial^3 \psi_2}{\partial x^2\partial y})-2A_{00}\frac{\partial^4 w}{\partial x^2\partial y^2}+J_{00}(\frac{\partial^3 \psi_1}{\partial x\partial y^2}-\frac{\partial^4 \psi_3}{\partial x^2\partial y^2})\\
&-A_{00}\frac{\partial^4 w}{\partial y^4}-\frac{1}{2}J_{00}(\frac{\partial^4 \psi_3}{\partial y^4}-\frac{\partial^3 \psi_2}{\partial y^3}+\frac{\partial^3 \psi_1}{\partial x\partial y^2}-\frac{\partial^4 \psi_3}{\partial x^2\partial y^2})+A_{00}\frac{\partial^4 w}{\partial x^2\partial y^2}\\
&+A_{00}\frac{\partial^4 w}{\partial x^2\partial y^2}+\frac{1}{2}J_{00}(\frac{\partial^4 \psi_3}{\partial x^2\partial y^2}-\frac{\partial^3 \psi_2}{\partial x^2\partial y}+\frac{\partial^3 \psi_1}{\partial x^3}-\frac{\partial^4 \psi_3}{\partial x^4})-A_{00}\frac{\partial^4 w}{\partial x^4}-q\\
&=I_1\frac{\partial^2 w}{\partial t^2}+I_2(\frac{\partial^3 u}{\partial x\partial t^2}+\frac{\partial^3 v}{\partial y\partial t^2})-I_3(\frac{\partial^4 w}{\partial x^2\partial t^2}+\frac{\partial^4 w}{\partial y^2\partial t^2})+I_5(\frac{\partial^3 \psi_1}{\partial x\partial t^2}+\frac{\partial^3 \psi_2}{\partial y\partial t^2})+I_7\frac{\partial^2 \psi_3}{\partial t^2},
\end{aligned}
\tag{A3}
$$

$$
\begin{aligned}
&D_{11}\frac{\partial^2 u}{\partial x^2}-G_{11}\frac{\partial^3 w}{\partial x^3}+K_{11}\frac{\partial^2 \psi_1}{\partial x^2}+D_{12}\frac{\partial^2 v}{\partial x\partial y}-G_{12}\frac{\partial^3 w}{\partial x\partial y^2}+K_{12}\frac{\partial^2 \psi_2}{\partial x\partial y}+L_{13}\frac{\partial \psi_3}{\partial x}\\
&+D_{66}(\frac{\partial^2 u}{\partial y^2}+\frac{\partial^2 v}{\partial x\partial y})-2G_{66}\frac{\partial^3 w}{\partial x\partial y^2}+K_{66}(\frac{\partial^2 \psi_2}{\partial x\partial y}+\frac{\partial^2 \psi_1}{\partial y^2})-N_{55}(\psi_1+\frac{\partial \psi_3}{\partial x})\\
&+\frac{1}{2}\left\{-2J_{00}\frac{\partial^3 w}{\partial x\partial y^2}+N_{00}(\frac{\partial^2 \psi_1}{\partial y^2}-\frac{\partial^3 \psi_3}{\partial x\partial y^2})\right\}-\frac{1}{2}\left\{N_{00}(\frac{\partial^2 \psi_2}{\partial x\partial y}-\frac{\partial^2 \psi_1}{\partial y^2})\right\}\\
&+\frac{1}{2}\left\{J_{00}\frac{\partial^3 w}{\partial x\partial y^2}+\frac{1}{2}N_{00}(\frac{\partial^3 \psi_3}{\partial x\partial y^2}-\frac{\partial^2 \psi_2}{\partial x\partial y}+\frac{\partial^2 \psi_1}{\partial x^2}-\frac{\partial^3 \psi_3}{\partial x^3})-J_{00}\frac{\partial^3 w}{\partial x^3}\right\}\\
&+\frac{1}{4}\left\{L_{00}(\frac{\partial^3 \psi_3}{\partial x\partial y^2}-\frac{\partial^2 \psi_2}{\partial x\partial y})+D_{00}(\frac{\partial^4 v}{\partial x^3\partial y}-\frac{\partial^4 u}{\partial x^2\partial y^2})+K_{00}(\frac{\partial^4 \psi_2}{\partial x^3\partial y}-\frac{\partial^4 \psi_1}{\partial x^2\partial y^2})\right\}\\
&+\frac{1}{4}\left\{L_{00}(\frac{\partial^2 \psi_1}{\partial y^2}-\frac{\partial^3 \psi_3}{\partial x\partial y^2})+D_{00}(\frac{\partial^4 v}{\partial x\partial y^3}-\frac{\partial^4 u}{\partial y^4})+K_{00}(\frac{\partial^4 \psi_2}{\partial x\partial y^3}-\frac{\partial^4 \psi_1}{\partial y^4})\right\}\\
&-\frac{1}{4}\left\{M_{00}(\psi_1-\frac{\partial \psi_3}{\partial x})+E_{00}(\frac{\partial^2 v}{\partial x\partial y}-\frac{\partial^2 u}{\partial y^2})+L_{00}(\frac{\partial^2 \psi_2}{\partial x\partial y}-\frac{\partial^2 \psi_1}{\partial y^2})\right\}\\
&=I_4\frac{\partial^2 u}{\partial t^2}-I_5\frac{\partial^3 w}{\partial x\partial t^2}+I_6\frac{\partial^2 \psi_1}{\partial t^2},
\end{aligned}
\tag{A4}
$$

$$
\begin{aligned}
&+D_{21}\frac{\partial^2 u}{\partial x\partial y}-G_{21}\frac{\partial^3 w}{\partial x^2\partial y}+K_{21}\frac{\partial^2 \psi_1}{\partial x\partial y}+D_{22}\frac{\partial^2 v}{\partial y2}-G_{22}\frac{\partial^3 w}{\partial y^3}+K_{22}\frac{\partial^2 \psi_2}{\partial y^2}+L_{23}\frac{\partial \psi_3}{\partial y}\\
&+D_{66}(\frac{\partial^2 u}{\partial x\partial y}+\frac{\partial^2 v}{\partial x^2})-2G_{66}\frac{\partial^3 w}{\partial x^2\partial y}+K_{66}(\frac{\partial^2 \psi_2}{\partial x^2}+\frac{\partial^2 \psi_1}{\partial x\partial y})-N_{44}(\psi_2+\frac{\partial \psi_3}{\partial y})\\
&-\frac{1}{2}\left\{2J_{00}\frac{\partial^3 w}{\partial x^2\partial y}+N_{00}(\frac{\partial^3 \psi_3}{\partial x^2\partial y}-\frac{\partial^2 \psi_2}{\partial x^2})\right\}+\frac{1}{2}\left\{N_{00}(\frac{\partial^2 \psi_2}{\partial x^2}-\frac{\partial^2 \psi_1}{\partial x\partial y})\right\}\\
&-\frac{1}{2}\left\{J_{00}\frac{\partial^3 w}{\partial y^3}+\frac{1}{2}N_{00}(\frac{\partial^3 \psi_3}{\partial y^3}-\frac{\partial^2 \psi_2}{\partial y^2}+\frac{\partial^2 \psi_1}{\partial x\partial y}-\frac{\partial^3 \psi_3}{\partial x^2\partial y})-J_{00}\frac{\partial^3 w}{\partial x^2\partial y}\right\}\\
&-\frac{1}{4}\left\{L_{00}(\frac{\partial^3 \psi_3}{\partial x^2\partial y}-\frac{\partial^2 \psi_2}{\partial x^2})+D_{00}(\frac{\partial^4 v}{\partial x^4}-\frac{\partial^4 u}{\partial x^3\partial y})+K_{00}(\frac{\partial^4 \psi_2}{\partial x^4}-\frac{\partial^4 \psi_1}{\partial x^3\partial y})\right\}\\
&-\frac{1}{4}\left\{L_{00}(\frac{\partial^2 \psi_1}{\partial x\partial y}-\frac{\partial^3 \psi_3}{\partial x^2\partial y})+D_{00}(\frac{\partial^4 v}{\partial x^2\partial y^2}-\frac{\partial^4 u}{\partial x\partial y^3})+K_{00}(\frac{\partial^4 \psi_2}{\partial x^2\partial y^2}-\frac{\partial^4 \psi_1}{\partial x\partial y^3})\right\}\\
&+\frac{1}{4}\left\{M_{00}(\frac{\partial \psi_3}{\partial y}-\psi_2)+E_{00}(\frac{\partial^2 v}{\partial x^2}-\frac{\partial^2 u}{\partial x\partial y})+L_{00}(\frac{\partial^2 \psi_2}{\partial x^2}-\frac{\partial^2 \psi_1}{\partial x\partial y})\right\}\\
&=I_4\frac{\partial^2 v}{\partial t^2}-I_5\frac{\partial^3 w}{\partial y\partial t^2}+I_6\frac{\partial^2 \psi_2}{\partial t^2},
\end{aligned}
\tag{A5}
$$

$$
\begin{aligned}
&-E_{31}\frac{\partial u}{\partial x}+H_{31}\frac{\partial^2 w}{\partial x^2}-L_{31}\frac{\partial \psi_1}{\partial x}-E_{32}\frac{\partial v}{\partial y}+H_{32}\frac{\partial^2 w}{\partial y^2}-L_{32}\frac{\partial \psi_2}{\partial y}-M_{33}\psi_3\\
&+N_{55}(\frac{\partial \psi_1}{\partial x}+\frac{\partial^2 \psi_3}{\partial x^2})+N_{44}(\frac{\partial \psi_2}{\partial y}+\frac{\partial^2 \psi_3}{\partial y^2})-\frac{1}{2}\left\{2J_{00}\frac{\partial^4 w}{\partial x^2\partial y^2}+N_{00}(\frac{\partial^4 \psi_3}{\partial x^2\partial y^2}-\frac{\partial^3 \psi_2}{\partial x^2\partial y})\right\}+\frac{\partial^3 \psi_1}{\partial x\partial y^2}-\frac{\partial^4 \psi_3}{\partial x^2\partial y^2})-J_{00}\frac{\partial^4 w}{\partial x^2\partial y^2}\Big\}+\frac{1}{2}\Big\{J_{00}\frac{\partial^4 w}{\partial x^2\partial y^2}+\frac{1}{2}N_{00}(\frac{\partial^4 \psi_3}{\partial x^2\partial y^2}-\frac{\partial^3 \psi_2}{\partial x^2\partial y}+\frac{\partial^3 \psi_1}{\partial x^3}-\frac{\partial^4 \psi_3}{\partial x^4})-\\
&+\frac{1}{2}\left\{-2J_{00}\frac{\partial^4 w}{\partial x^2\partial y^2}+N_{00}(\frac{\partial^3 \psi_1}{\partial x\partial y^2}-\frac{\partial^4 \psi_3}{\partial x^2\partial y^2})\right\}\\
&-\frac{1}{2}\left\{J_{00}\frac{\partial^4 w}{\partial y^4}+\frac{1}{2}N_{00}(\frac{\partial^4 \psi_3}{\partial y^4}-\frac{\partial^3 \psi_2}{\partial y^3}\right.
\end{aligned}
\tag{A6}
$$

in which

$$
\begin{aligned}
A_{ij} &= \int_{-\frac{h}{2}}^{\frac{h}{2}} Q_{ij} dz \\
B_{ij} &= \int_{-\frac{h}{2}}^{\frac{h}{2}} z Q_{ij} dz \\
D_{ij} &= \int_{-\frac{h}{2}}^{\frac{h}{2}} f(z) Q_{ij} dz \\
E_{ij} &= \int_{-\frac{h}{2}}^{\frac{h}{2}} f^{''}(z) Q_{ij} dz \\
F_{ij} &= \int_{-\frac{h}{2}}^{\frac{h}{2}} z^2 Q_{ij} dz \\
G_{ij} &= \int_{-\frac{h}{2}}^{\frac{h}{2}} z f(z) Q_{ij} dz \\
H_{ij} &= \int_{-\frac{h}{2}}^{\frac{h}{2}} z f^{''}(z) Q_{ij} dz \\
K_{ij} &= \int_{-\frac{h}{2}}^{\frac{h}{2}} f^2(z) Q_{ij} dz \\
L_{ij} &= \int_{-\frac{h}{2}}^{\frac{h}{2}} f(z) f^{''}(z) Q_{ij} dz \\
M_{ij} &= \int_{-\frac{h}{2}}^{\frac{h}{2}} f^{''}(z) f^{''}(z) Q_{ij} dz \\
N_{ij} &= \int_{-\frac{h}{2}}^{\frac{h}{2}} f^{'}(z) f^{'}(z) Q_{ij} dz \\
A_{00} &= \int_{-\frac{h}{2}}^{\frac{h}{2}} \left(\frac{E(z)\ell^2}{2+2\nu}\right) dz \\
D_{00} &= \int_{-\frac{h}{2}}^{\frac{h}{2}} f(z) \left(\frac{E(z)\ell^2}{2+2\nu}\right) dz \\
E_{00} &= \int_{-\frac{h}{2}}^{\frac{h}{2}} f^{''}(z) \left(\frac{E(z)\ell^2}{2+2\nu}\right) dz \\
J_{00} &= \int_{-\frac{h}{2}}^{\frac{h}{2}} f^{'}(z) \left(\frac{E(z)\ell^2}{2+2\nu}\right) dz \\
K_{00} &= \int_{-\frac{h}{2}}^{\frac{h}{2}} f^2(z) \left(\frac{E(z)\ell^2}{2+2\nu}\right) dz \\
L_{00} &= \int_{-\frac{h}{2}}^{\frac{h}{2}} f(z) f^{''}(z) \left(\frac{E(z)\ell^2}{2+2\nu}\right) dz \\
M_{00} &= \int_{-\frac{h}{2}}^{\frac{h}{2}} f^{''}(z) f^{''}(z) \left(\frac{E(z)\ell^2}{2+2\nu}\right) dz \\
N_{00} &= \int_{-\frac{h}{2}}^{\frac{h}{2}} f^{'}(z) f^{'}(z) \left(\frac{E(z)\ell^2}{2+2\nu}\right) dz
\end{aligned}
\tag{A7}
$$

References

[1] Jena SK, Chakraverty S, Mahesh V, Harursampath D. Application of Haar wavelet discretization and differential quadrature methods for free vibration of functionally graded micro-beam with porosity using modified couple stress theory. Eng Anal Bound Elem 2022;140:167–85.

[2] Ghayesh MH, Farokhi H, Amabili M. Nonlinear behaviour of electrically actuated MEMS resonators. Int J Eng Sci 2013;71:137–55.

[3] Pillai G, Li S-S. Piezoelectric MEMS resonators: A review. IEEE Sens J 2020;21:12589–605.

[4] Morkvenaite-Vilkonciene I, Bucinskas V, Subaciute-Zemaitiene J, Sutinys E, Virzonis D, Dzedzickis A. Development of electrostatic microactuators: 5-year progress in modeling, design, and applications. Micromachines 2022;13:1256.

[5] Yang W, Liu M, Chen S, Kang W, Chen J, Li Y. Electromechanical analysis of a self-sensing torsional micro-actuator based on CNTs reinforced piezoelectric composite with damage. Compos Struct 2023;313:116945.

[6] Mahmud MP, Bazaz SR, Dabiri S, Mehrizi AA, Asadnia M, Warkiani ME, et al. Advances in mems and microfluidics-based energy harvesting technologies. Advanced Materials Technologies 2022;7:2101347.

[7] Wang X, Wu S, Yin J, Moradi Z, Safa M, Khadimallah MA. On the electromechanical energy absorption of the reinforced composites piezoelectric MEMS via Adaptive neuro-fuzzy inference system and MCS theory. Compos Struct 2023;303:116246.

[8] Gao W, Qiao Z, Han X, Wang X, Shakoor A, Liu C, et al. A MEMS micro force sensor based on a laterally movable gate field-effect transistor (LMGFET) with a novel decoupling sandwich structure. Engineering 2023;21:61–74.

[9] Fang W, Li S-S, Li M-H. Leveraging semiconductor ecosystems to MEMS. In: 2023 IEEE 36th International Conference on Micro Electro Mechanical Systems. (MEMS): IEEE; 2023. p. 143–8.
[10] Duffy S, Bozler C, Rabe S, Knecht J, Travis L, Wyatt P, et al. MEMS microswitches for reconfigurable microwave circuitry. IEEE Microwave Wirel Compon Lett 2001; 11:106–8.
[11] López-Tapia A, Mares-Carreño J, Abarca-Jiménez GS, Reyes-Barranca MA. Design and simulation of a closed loop controlled linear displacement MEMS micromotor, based on a floating gate transistor. SILICON 2023;1–14.
[12] Seymour JP, Wu F, Wise KD, Yoon E. State-of-the-art MEMS and microsystem tools for brain research. Microsyst Nanoeng 2017;3:1–16.
[13] Receveur RA, Lindemans FW, De Rooij NF. Microsystem technologies for implantable applications. J Micromech Microeng 2007;17:R50.
[14] Feizi S, Cooksley CM, Nepal R, Psaltis AJ, Wormald P-J, Vreugde S. Silver nanoparticles as a bioadjuvant of antibiotics against biofilm-mediated infections with methicillin-resistant Staphylococcus aureus and Pseudomonas aeruginosa in chronic rhinosinusitis patients. Pathology 2022;54:453–9.
[15] Bakeer B, Elsabbagh A, Hedaya M. Design of micro-plates subjected to residual stresses in microelectromechanical systems (MEMS) applicationss. Port-Said Engineering Research Journal 2021;25:165–9.
[16] Caruntu DI, Oyervides R. Amplitude–frequency response of parametric resonance of electrostatically actuated MEMS clamped circular plate. Int J Non Linear Mech 2023;149:104310.
[17] Witvrouw A, Mehta A. The use of functionally graded poly-SiGe layers for MEMS applications. Materials science forum: Trans Tech Publ; 2005. p. 255–60.
[18] Ghayesh MH, Farokhi H. Nonlinear behaviour of electrically actuated microplate-based MEMS resonators. Mech Syst Sig Process 2018;109:220–34.
[19] Jia X, Ke L, Zhong X, Sun Y, Yang J, Kitipornchai S. Thermal-mechanical-electrical buckling behavior of functionally graded micro-beams based on modified couple stress theory. Compos Struct 2018;202:625–34.
[20] Hasan M, Zhao J, Jiang Z. Micromanufacturing of composite materials: a review. International Journal of Extreme Manufacturing 2019;1:012004.
[21] Jha D, Kant T, Singh R. A critical review of recent research on functionally graded plates. Compos Struct 2013;96:833–49.
[22] Mahi A, Tounsi A. A new hyperbolic shear deformation theory for bending and free vibration analysis of isotropic, functionally graded, sandwich and laminated composite plates. App Math Model 2015;39:2489–508.
[23] Zheng Y, Karami B, Shahsavari D. On the vibration dynamics of heterogeneous panels under arbitrary boundary conditions. Int J Eng Sci 2022;178:103727.
[24] Caruntu DI. Classical Jacobi polynomials, closed-form solutions for transverse vibrations. J Sound Vib 2007;306:467–94.
[25] Caruntu DI. Dynamic modal characteristics of transverse vibrations of cantilevers of parabolic thickness. Mech Res Commun 2009;36:391–404.
[26] Bohidar SK, Sharma R, Mishra PR. Functionally graded materials: A critical review. International Journal of Research 2014;1:289–301.
[27] Li Y, Feng Z, Hao L, Huang L, Xin C, Wang Y, et al. A review on functionally graded materials and structures via additive manufacturing: from multi-scale design to versatile functional properties. Advanced Materials Technologies 2020;5:1900981.
[28] Thanh CL, Nguyen TN, Vu TH, Khatir S, Abdel WM. A geometrically nonlinear size-dependent hypothesis for porous functionally graded micro-plate. Eng Comput 2020;1–12.
[29] Shahmohammadi MA, Mirfatah SM, Salehipour H, Civalek Ö. On nonlinear forced vibration of micro scaled panels. Int J Eng Sci 2023;182:103774.
[30] Karami B, Ghayesh MH. Vibration characteristics of sandwich microshells with porous functionally graded face sheets. Int J Eng Sci 2023;189:103884.
[31] Tocci Monaco G, Fantuzzi N, Fabbrocino F, Luciano R. Trigonometric solution for the bending analysis of magneto-electro-elastic strain gradient nonlocal nanoplates in hygro-thermal environment. Mathematics 2021;9:567.
[32] Tocci Monaco G, Fantuzzi N, Fabbrocino F, Luciano R. Critical temperatures for vibrations and buckling of magneto-electro-elastic nonlocal strain gradient plates. Nanomaterials 2021;11:87.
[33] Garg A, Mukhopadhyay T, Belarbi M, Chalak H, Singh A, Zenkour A. On accurately capturing the through-thickness variation of transverse shear and normal stresses for composite beams using FSDT coupled with GPR. Compos Struct 2023;305: 116551.
[34] Dastjerdi S, Naeijian F, Akgöz B, Civalek Ö. On the mechanical analysis of microcrystalline cellulose sheets. Int J Eng Sci 2021;166:103500.
[35] Li Y, Xiao T. Free vibration of the one-dimensional piezoelectric quasicrystal microbeams based on modified couple stress theory. App Math Model 2021;96: 733–50.
[36] Malikan M, Eremeyev VA. On time-dependent nonlinear dynamic response of micro-elastic solids. Int J Eng Sci 2023;182:103793.
[37] Zhu J, Lai Z, Yin Z, Jeon J, Lee S. Fabrication of ZrO2–NiCr functionally graded material by powder metallurgy. Mater Chem Phys 2001;68:130–5.
[38] Wattanasakulpong N, Prusty BG, Kelly DW, Hoffman M. Free vibration analysis of layered functionally graded beams with experimental validation. Mater Des 2012; 36:182–90.
[39] Wattanasakulpong N, Chaikittiratana A. Flexural vibration of imperfect functionally graded beams based on Timoshenko beam theory: Chebyshev collocation method. Meccanica 2015;50:1331–42.
[40] Kumar R, Lal A, Singh B, Singh J. Meshfree approach on buckling and free vibration analysis of porous FGM plate with proposed IHHSDT resting on the foundation. Curved and Layered Structures 2019;6:192–211.
[41] Rezaei A, Saidi A, Abrishamdari M, Mohammadi MP. Natural frequencies of functionally graded plates with porosities via a simple four variable plate theory: An analytical approach. Thin-Walled Struct 2017;120:366–77.
[42] Kumar V, Singh S, Saran VH, Harsha SP. Vibration characteristics of porous FGM plate with variable thickness resting on Pasternak's foundation. European Journal of Mechanics-A/Solids 2021;85:104124.
[43] Su J, He W, Zhang K, Zhang Q, Qu Y. Vibration analysis of functionally graded porous cylindrical shells filled with dense fluid using an energy method. App Math Model 2022;108:167–88.
[44] Su J, He W, Zhou K. Study on vibration behavior of functionally graded porous material plates immersed in liquid with general boundary conditions. Thin-Walled Struct 2023;182:110166.
[45] Zhang Y, Jin G, Chen M, Ye T, Yang C, Yin Y. Free vibration and damping analysis of porous functionally graded sandwich plates with a viscoelastic core. Compos Struct 2020;244:112298.
[46] Liang C, Wang YQ. A quasi-3D trigonometric shear deformation theory for wave propagation analysis of FGM sandwich plates with porosities resting on viscoelastic foundation. Compos Struct 2020;247:112478.
[47] Akbaş ŞD, Fageehi Y, Assie A, Eltaher M. Dynamic analysis of viscoelastic functionally graded porous thick beams under pulse load. Eng Comput 2022;1–13.
[48] Allah MJ, Timesli A. Nonlinear dynamic analysis of viscoelastic FGM with linear and nonlinear porosity distributions. Materials Today. Communications 2023.
[49] Shojaeefard MH, Googarchin HS, Ghadiri M, Mahinzare M. Micro temperature-dependent FG porous plate: Free vibration and thermal buckling analysis using modified couple stress theory with CPT and FSDT. App Math Model 2017;50: 633–55.
[50] Mirjavadi SS, Afshari BM, Barati MR, Hamouda A. Strain gradient based dynamic response analysis of heterogeneous cylindrical microshells with porosities under a moving load. Mater Res Express 2018;6:035029.
[51] Phung-Van P, Thai CH, Nguyen-Xuan H, Wahab MA. Porosity-dependent nonlinear transient responses of functionally graded nanoplates using isogeometric analysis. Compos B Eng 2019;164:215–25.
[52] Chen S-X, Sahmani S, Safaei B. Size-dependent nonlinear bending behavior of porous FGM quasi-3D microplates with a central cutout based on nonlocal strain gradient isogeometric finite element modelling. Eng Comput 2021;37:1657–78.
[53] Guo L, Xin X, Shahsavari D, Karami B. Dynamic response of porous E-FGM thick microplate resting on elastic foundation subjected to moving load with acceleration. Thin-Walled Struct 2022;173:108981.
[54] Farokhi H, Ghayesh MH. Viscoelastic resonant responses of shear deformable imperfect microbeams. J Vib Control 2018;24:3049–62.
[55] Jalaei M, Civalek Ö. On dynamic instability of magnetically embedded viscoelastic porous FG nanobeam. Int J Eng Sci 2019;143:14–32.
[56] Liu G, Wu S, Shahsavari D, Karami B, Tounsi A. Dynamics of imperfect inhomogeneous nanoplate with exponentially-varying properties resting on viscoelastic foundation. European J Mechanics-A/Solids 2022;95:104649.
[57] Ghayesh MH, Farokhi H. Nonlinear dynamics of microplates. Int J Eng Sci 2015;86: 60–73.
[58] Ghayesh MH. Nonlinear dynamics of multilayered microplates. J Comput Nonlinear Dyn 2018;13.
[59] Kim J, Żur KK, Reddy J. Bending, free vibration, and buckling of modified couples stress-based functionally graded porous micro-plates. Compos Struct 2019;209: 879–88.
[60] Akavci S, Tanrikulu A. Static and free vibration analysis of functionally graded plates based on a new quasi-3D and 2D shear deformation theories. Compos B Eng 2015;83:203–15.
[61] Zenkour A. Benchmark trigonometric and 3-D elasticity solutions for an exponentially graded thick rectangular plate. Arch Appl Mech 2007;77:197–214.
[62] Matsunaga H. Free vibration and stability of functionally graded plates according to a 2-D higher-order deformation theory. Compos Struct 2008;82:499–512.
[63] Carrera E, Brischetto S, Cinefra M, Soave M. Effects of thickness stretching in functionally graded plates and shells. Compos B Eng 2011;42:123–33.
[64] Yang F, Chong A, Lam DCC, Tong P. Couple stress based strain gradient theory for elasticity. Int J Solids Struct 2002;39:2731–43.
[65] Lam DC, Yang F, Chong A, Wang J, Tong P. Experiments and theory in strain gradient elasticity. J Mech Phys Solids 2003;51:1477–508.
[66] Reddy J, Kim J. A nonlinear modified couple stress-based third-order theory of functionally graded plates. Compos Struct 2012;94:1128–43.
[67] ANSYS® MultiphysicsTM. Workbench 19.2, Workbench User's Guide, ANSYS Workbench Systems Analysis Systems, Modal 2022.
[68] Srinivas S, Rao CJ, Rao A. An exact analysis for vibration of simply-supported homogeneous and laminated thick rectangular plates. J Sound Vib 1970;12: 187–99.
[69] Jha D, Kant T, Singh R. Free vibration response of functionally graded thick plates with shear and normal deformations effects. Compos Struct 2013;96:799–823.
[70] Benahmed A, Houari MSA, Benyoucef S, Belakhdar K, Tounsi A. A novel quasi-3D hyperbolic shear deformation theory for functionally graded thick rectangular plates on elastic foundation. Geomechanics and Engineering 2017;12:9–34.
[71] Thai H-T, Choi D-H. Size-dependent functionally graded Kirchhoff and Mindlin plate models based on a modified couple stress theory. Compos Struct 2013;95: 142–53.
[72] Jung W-Y, Park W-T, Han S-C. Bending and vibration analysis of S-FGM microplates embedded in Pasternak elastic medium using the modified couple stress theory. Int J Mech Sci 2014;87:150–62.
[73] Papargyri-Beskou S, Beskos D. Static, stability and dynamic analysis of gradient elastic flexural Kirchhoff plates. Arch Appl Mech 2008;78:625–35.